Ph.D Dissertation

Anion detection in air using silicon nanoFET

실리콘 나노전계효과트랜지스터를 이용한

공기중 음이온의 측정

2016 년 2 월

서울대학교 대학원

전기 컴퓨터 공학부

서 영 태

Anion detection in air using silicon nanoFET

실리콘 나노전계효과트랜지스터를 이용한 공기중 음이온의 측정

지도교수 김 용 권

이 논문을 공학박사 학위논문으로 제출함

2016 년 2 월

서울대학교 대학원
전기 컴퓨터 공학부
서 영 태

서영태의 공학박사 학위논문을 인준함

2016 년 2 월

위 원 장 _____ 이 윤 식 (인)

부위원장 _____ 김 용 권 (인)

위 원 _____ 정 대 홍 (인)

위 원 _____ 김 성 재 (인)

위 원 _____ 성 우 경 (인)

Abstract

This study aims to produce a nano-field-effect-transistor (nanoFET) with a top-down approach, and quantitatively determine the concentration of negative ions in the air. The operational principles of this device are experimentally evaluated, by measuring the changes in channel conductance caused by the field-effect generated on the device's nanochannel by electric charges. The development of such sensors has been hindered by various noise signals occurring in nanoFET experiments, including interference caused by ion concentration, pH, and the electrical potential of the buffer solution. The measurement of airborne anions using nanoFETs, the approach proposed in this study, can be clearly explained in terms of the chemical gate phenomenon, a phenomenon caused by the adsorption of electrically charged particles. Moreover, by evaluating the performance of existing commercial devices to measure airborne anion levels, the possibility was investigated in commercializing the nanoFET-based airborne anion sensor.

The existing methods to measure airborne anions detect changes in electric fields, caused by the negative charged particles in the air, using Gerdien tubes, and air ventilators to draw air into the tubes. Commercial airborne anion measurement devices using Gerdien tubes have larger sizes then nanoFET-based solutions, Moreover, it is difficult to integrate those devices with air ionizers (that produce anions), which have recently started to be used in many aspects of everyday life, or with air quality related devices. In contrast, the nanoFET-based anion measurement system can be integrated with anion suppliers in small home appliances, such as air purifiers, electric fans, and refrigerators; this system can therefore be used as an indicator, to effectively control airborne anions, manage air quality, and sustain healthy living conditions.

Other studies address the manufacturing process. In the beginning, this research was focused on the fundamental characteristics of nanoFETs, including the electrical characteristics of nanowires and CNT; therefore, studies were conducted to confirm the possibility of developing nanoFET sensors with a bottom-up approach. In contrast to this early nanoFET research, studies are currently focused on reproducible manufacturing methods, capable of enabling mass production of nanoFETs for commercial nanoFET device development. Even in devices using outstanding single-walled carbon nanotubes (SWCNT) or single crystal nanowires, the productivity of the bottom-up approach declines in comparison with the top-down approach, when structures are dispersed on wafers and electrodes are formed. Recently, a strong desire to obtain better controlled device characteristics at wafer scale led to a top-down approach using conventional microfabrication processes to create nanowire-like structures. Until now, research on the top-down approach has focused on the uniformity of the nanochannel length and the reproducibility of signals, by first producing nanowire structures according to the crystal orientation of the silicon wafer through a wet-etching process, and then producing source, drain, and gate electrodes. However, even devices produced with this conventional top-down approach have problems to overcome; the manufacturing process is difficult, and thus not suitable for the production of commercial sensors, and its production yield should also be improved.

In this study, the complex nanoFET manufacturing process is simplified, using a typical microelectromechanical system (MEMS) process to enable mass production, by implementing a batch process for nanoFET channel placement on 8-inch ultra-thin silicon-on-insulator (UT-SOI) wafers, up to surface treatment. The nanochannel, gate oxide, floating gate electrode (Ti/Au), and buried oxide (BOX) silicon layer were 20, 15, 10/100, and 145 nm, respectively. The length and width of the channels were 5 μm and 1 μm, respectively. The obtained results confirmed the chemical gate phenomenon,

caused by the adsorption of electrically charged particles to the channels of the nanoFET. By measuring the operational characteristics of the nanoFET repeatedly, in different air anionic concentrations, it was clearly demonstrated that the electric charges adsorbed onto the channel surface operated via the chemical gate phenomenon. For quantitative analysis, the change was measured the change in the gradient of the drain-source electric current (Ids), which occurs when the anions produced by anion ionizers diffuse into the air and adsorb onto the gate surface, and acts, therefore, as the device detection parameter. Moreover, the introduction of an additional gold top-gate electrode on top of the gate oxide film of the nanoFET, not only increased the size of the detector, but also provided a mechanism to reinitialize the accumulation of charges, thus improving the efficiency of the nanoFET as an airborne anion sensor. These results lead us to believe that nanoFET sensors with a top-gate electrode will find efficient applications as airborne anion measurement sensors. It was expected that the understanding of the operational principles of nanoFET devices produced by these basic experimental results will help solve the problems that are currently preventing the use of nanoFETs as biosensors.

Keywords: Negative ions in air, Quantitative detection of anions, nanoFET, Chemical gate, Conductance change rate, MEMS

Student Number: 2007-30828

Contents

List of Figures

List of Tables

Chapter 1.
Introduction

1.1 Introduction

Since the late 1990s, nanodevice application techniques using carbon nanotubes (CNT) or nanowires have received widespread interest. Several areas—including nanosubstance synthesis techniques [1-5], device production, assembly, and integration techniques [4, 6, 7], and techniques for production of electric circuits, have continuously gained notice and been the subject of much research, due to the structural advantages, semiconductive properties, and low power consumption of nano-sized devices. In the beginning, research was focused on the fundamental characteristics of nano-field-effect-transistors (nanoFETs), including the electrical characteristics of nanowires and CNT. Two major trends exist today among researchers, with continuous reports of studies in the two following areas: the manufacturing process of nanoFET devices, and the physical characteristics of these devices. The first area (manufacturing process) can further be divided into a bottom-up approach and a top-down approach. In the bottom-up approach, electrodes are formed by synthesizing CNT or single crystal nanowires with relatively good electrical properties, and these electrodes are then applied to devices. This approach has been

investigated through many studies since the early phases of research, and multiple studies have reported the advantages of using bottom-up produced nanoFET devices as sensors. However, the bottom-up approach has low productivity, due to device uniformity and the complexity of the manufacturing process; therefore, the top-down approach has recently been gaining attention. In the second mentioned area (research on the physical characteristics of devices), studies are being conducted to elucidate performance metrics and establish clear operating principles.

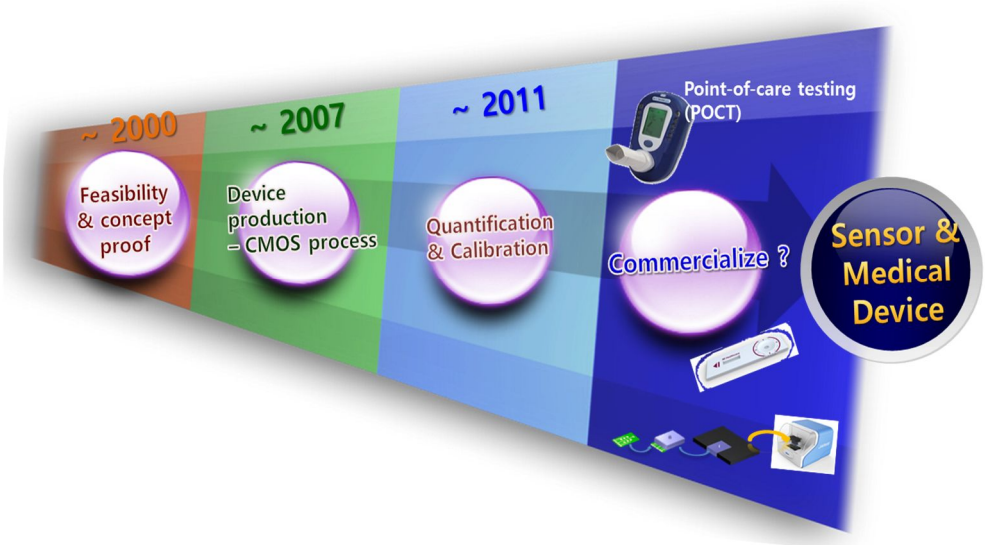

Figure 1. Research and development trends on nanoFETs.

NanoFETs were extensively studied, because of their advantage of being able to directly detect an unknown bioparticle through electric signals, and thus allow for real-time monitoring of analyte concentration changes, without requiring separate labeled substances or a labeling process [8-14]. Moreover, owing to the possibility of mass production of nanoFETs using semiconductor processes, many studies have now focused on identifying methods for employing nanoFET as biosensors [7-15].

Although the concept of using a nanoFET to directly detect the charge of a bioparticle by field effect is a simple one, its practical implementation is severely limited, because the measurement environment is often an electrolyte solution mixed with various ions, such as a physiological saline [16, 17]. The development of practical applications is hindered by problems such as the Debye screening effect (where the area of the electric field created by the bioparticle's charge reduces rapidly, depending on the ion concentration of the buffer solution), high sensitivity to the pH value of the sample solution (the actual measurement environment), and difficulties associated with the pI value (the charge of the bioparticle changes according to the pH of the solution); all these problems need to be considered [8, 17-21]. Furthermore, the electric potential applied to the solution affects the nanoFET channel and, therefore, this channel is affected by the electrode material when voltage is applied to the solution or a bias voltage is set [17].

The FET-based sensor

The FET-based sensor can be integrated and miniaturized based on established semiconductor processes, employing a label-free detection method to directly convert the electrical signal [2, 15, 19, 20, 22-28]. In general, a FET comprises source, drain, and gate electrodes. The amount of current flowing in the conducting membrane between drain and source is the electric element controlled by the gate. The conducting membrane formed between source and drain is a nanosized channel; therefore, the conductivity of the entire nanostructure can change significantly if even a low number of molecules or a minute amount of analysis material attaches to the gate membrane surface. Hence, it is not only simpler than FET-based biosensors, but also presents superior agility, convenience, accuracy, and durability. The gate current can be changed through chemical reactions without even applying voltage to the gate. The phenomenon through which charges affect the electric field of the nanochannel in such chemical reactions is called the chemical gate phenomenon [6, 15, 29-33]. This phenomenon can be used and applied to chemical sensors or biosensors. General FET-based sensors fix the receptor to the FET gate, to measure changes in the electrical signals generated when the receptor and the analysis material are coupled [11, 12, 28, 34, 35]. Actual examples are enzyme FETs that fix the enzyme to the

gate, the ImmunoFET using antigen and antibody reactions, and the ISFET, used as a pH sensor. These types of FET biosensors allow for real-time detection, miniaturization, and cost effectiveness, because they can be mass-produced with established semiconductor processes. However, nanowire reproducibility is a problem that must be solved for the actual implementation of FET biosensors. A difference in reproducibility implies a difference in sensitivity; extensive research will therefore be required, to create a nanowire with high reproducibility. Another problem is the high salt concentration of the analysis material; FET biosensors are highly sensitive to even the smallest salt concentration, and a buffer solution is thus used for detection, instead of directly measuring the sample [11, 15, 18-20].

Gate modulation in FETs

When a voltage is applied between source and drain, current will tend to flow between these two terminals. The intensity of this current can be controlled by applying a voltage to the gate, and thus, establishing an electric field in the gate region, through which the source to drain current will have to pass. Such a method of current control is called Gate Modulation. In other words, the electric current between two terminals of a

device can be controlled by an input voltage applied to a third terminal. The channel between the source and drain electrodes can be created with negative charges (electrons) or positive charges (positive charged ions), depending on the doping materials used in the nanoFET manufacture. A p-type FET—whose drain-source current channel is based on positive charges—was fabricated for the experiment.

The electric current between source and drain in the p-type FET, which depends of the voltage present in the gate (whose electric field is affected by negative charges) was measured. This is a label-free detection of the electrical conductance variations generated by changes in the electric charge of the channel, due to the action of target biomaterials attached to the surface of the gate electrode. Therefore, an inter-biomaterial binding on the surface of the nanoFET channel has similar effects to those of gate voltage. Gate modulation can thus be used for real-time measurements of electric current changes in the surface of FETs, depending on the size and type of electric charges induced on the surface of a channel or the immune response.

Anions in the air

Airborne ion density organized the fundamental monitored parameters of

the atmosphere [36]. Their influence on living organisms has been the subject of intensive studies. When the concentration of negative ions in the air increases, floating pollutants in the air will be supplied with electrons and thus become negatively charged particles. Ionized contaminants are attracted to each other, form ionized clusters, and sink to the floor surface. Figure 2 shows the air-purifying ability of anions. The existence of negative ions in air is of great interest, due to its air purification capabilities, and the positive effects resulting of healthier living conditions [37-41].

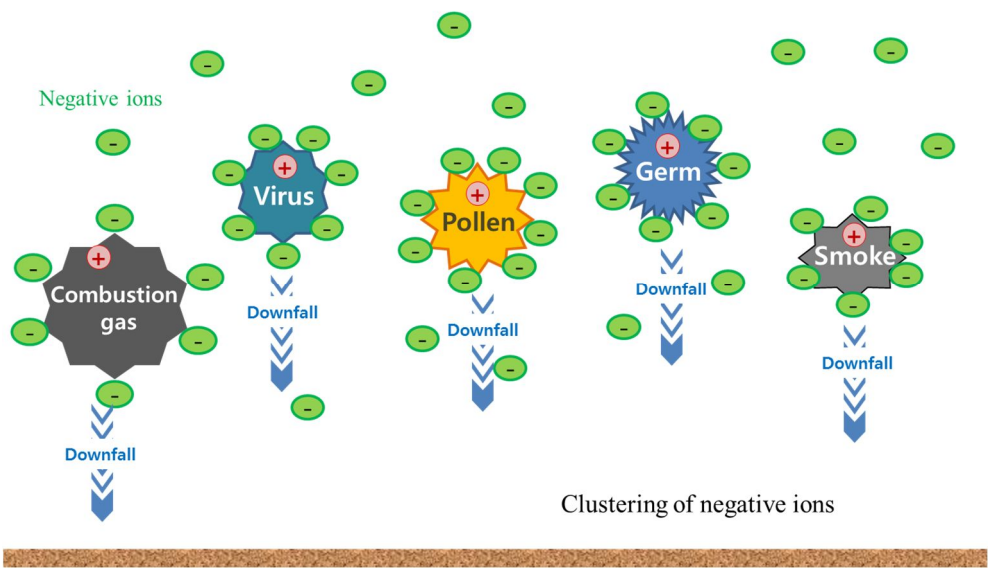

Figure 2. Purification effect of negative ions on indoors air corpuscles.

A considerable number of consumer products using ion-generating to remove airborne viruses, pollen, smoke, bacteria, and pollutants from breathing surrounding have become available [36, 42]. These devices work by generating a flow of anions in the air, which charge and bind together airborne particulate matter. Daily necessities have also been processed in various other ways, by artificially generating negative ions. The charged matter then gathers together and precipitates to the ground. Ion generating devices have been reported to be effective against combustion gas, dust, pollen, bacteria, and viruses. In addition to removing harmful particulates from the atmosphere, anions in the air also have a number of other health benefits [43, 44].

The physiological action of airborne ions on the human body can be seen in Table 1. A growing number of people are using personal and home air purification products to generate negative ions, thus charging and removing airborne particulate matter, and creating localized zones of improved air quality [45-47].

Table 1. Effects of airborne ions on the human body

Biological effects	Negative ions	Positive ions
Nerve stimulation	Parasympathetic nerve stimulation	Sympathetic nerve stimulation
Frame of mind	Satisfaction	Displeasure
Systemic organization	Sedation, Hypnosis	Stimulation, Excitement, Sleeplessness
Breath	Suppress	Promote
Oxygen Consumption	Decrease	Increase
Leukocyte	Decrease	Increase
Capillaries	Expansion	Contraction
Diuresis	Promote	Suppress
Pulse	Decrease	Increase
Blood pressure	Decrease	Increase

1.2 Background

A recently published report indicates that nanoFETs are potentially applicable as biosensors, due to their excellent electrical properties, and the chemical gating phenomena induced by the reaction between target biomaterial and the bioprobe, which supports their use in label-free methods [12-15, 20, 25, 26, 28, 32, 48]. NanoFETs created with a bottom-up approach are, however, difficult to produce commercially, because it is hard to produce devices with uniform characteristics [33, 49-52]. Despite their excellent applicability as biosensors, through surface reforming, and superb electrical properties and immune response, it is extremely difficult, in practice, to commercialize nanoFETs as biosensors. Therefore, the present study aims at finding a method to fabricate such devices with standard photolithography, with a top-down approach to the nanoFET's manufacturing process [8, 15, 27, 35, 51, 53]. With this approach, a mass production-enabled nanoFET was fabricated, and a FET based platform to sense anions in the air was developed.

Although several methods are used to measure airborne ion fields, most commercially available anion measurement equipment uses the Gerdien tube method, whose operating principle is shown in Figure 3.

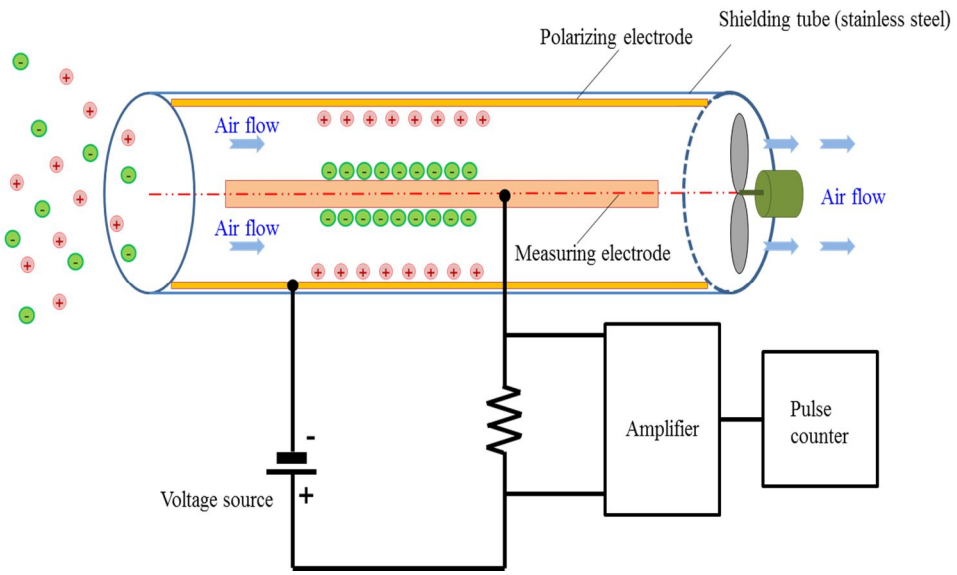

Figure 3. Anions in air detection principle of Gerdien tube method.

Various devices exist to detect airborne anions, including the Geiger-Muller tube based radiation detector, and parallel plate—or cylindrical plate —based electrostatic type detectors, with fans for airflow intake to the electrode plate detector [54-56]. The Gerdien tube consists of two electrodes to measure the current change. An electric field is applied between the core electrode inside the cylinder and the cylinder outer electrode in the figure 3. When the fan propelled air flows through the Gerdien tube, the airborne ions are exposed to the electric field created between the inner and outer electrodes, and the resulting Coulomb force forces them to move toward the

electrode of opposite charge sign. Airborne ions in the electric field collide with the inner electrode. So the resulting current is proportional to the ion concentration in the air. The measuring device is composed of a circuit section to measure the applied electric field, and an ion collecting section, to capture the airborne ions. These airborne ion counter devices are complicated systems, much larger and expensive than most ion generating devices. Commercially available airborne anion measuring instruments are, thus, difficult to integrate directly with other systems, and tend to occupy large volumes.

1.3 Motivation

The purpose of this study is twofold. Firstly, it aims to increase productivity of nanoFET device manufacturing, by comparing conventional devices made with a bottom-up approach with a few hundred nanometer-sized structures fabricated using a microelectromechanical system (MEMS) process, in a top-down approach. A large-scale nanoFET device was developed with photolithography, a method commonly used in semiconductor manufacturing processes. Secondly, this study aims to experimentally demonstrate—for the first time—the mechanism of chemical gating induced by adsorption of charged substances on a FET gate, by measuring the conductance change of a nanoFET used for anion detection in air [57].

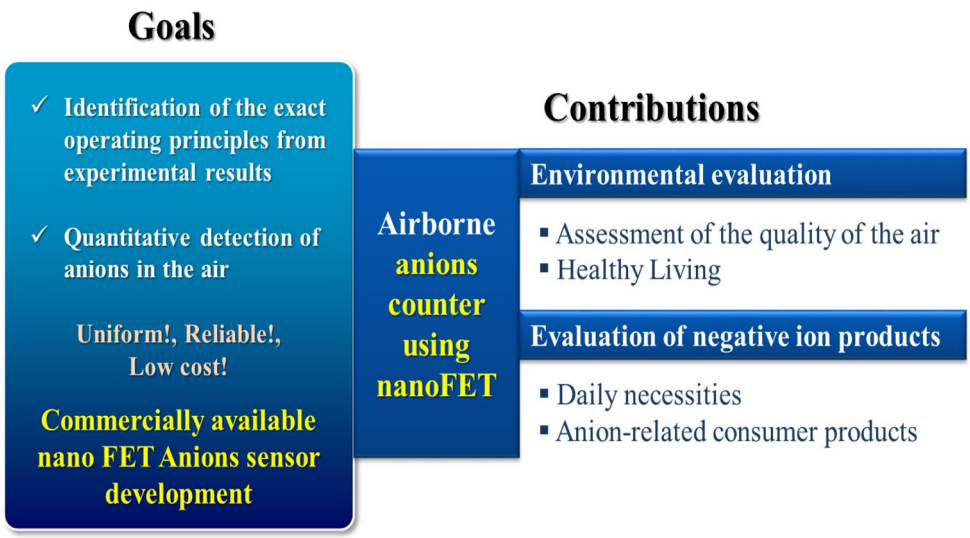

Figure 4. Diagrammatic representation of the research objectives and motivation.

The feasibility was also tested in a nano-field-effect-transistor (nanoFET) based sensor for detecting anions in the air. It was experimentally demonstrated that the air anionic concentration can be detected by evaluating the conductance variation in the nanoFET channel due to adsorption of charged particles on the sensor nanoFET's gate surface. From the anion detection experiments, the characteristics of chemical gating, the operating mechanism of the nanoFET biosensor, were measured. The pH solution potential and buffer ionic strength in air have minimal variations. Hence, the electric field-effect resulting from the adsorption of charged particles was easily measured, to characterize the movement of the field-effect transistor.

In this study, the operating mechanism was demonstrated for chemical gating by measuring and analyzing both the conductance variation and the response characteristics of the nano-field-effect channel, using various anionic concentrations in the air.

1.4 Document structure

In Chapter 2, this study explain both the nanoFET operating principle, and the limits to its usage as a general nanoFET sensor.

In Chapter 3, this study address the structure and design of the proposed nanoFET. This study also address its design and manufacturing; this study show that it can be mass produced with general MEMS processes using a silicon-on-insulator (SOI) wafer, and discuss its fabrication method.

In Chapter 4, this study present an experiment designed to verify the foundations of the nano FET operating principle (chemical gating), where the concentration of anions in the air is measured with the biosensor platform discussed in Chapter 3. In this experiment, this study first set the back-gate voltage range, based on the current-voltage characteristics of the developed nanoFET; this study then control the airborne anionic concentration, by controlling the distance to a commercial plasma-type ion generator. This study kept the gate voltage steady, and measured the airborne anionic concentration. A comparative explanation of the obtained results is presented in this Chapter.

Chapter 5 provides a final review of the study, and concludes this dissertation.

Chapter 2.
Chemical gating nanoFET

2.1 Introduction

Bio field-effect-transistor (BioFET) based studies have received glaring attention as a high potential line of research, because advances in processing technologies allow their mass production, and the compact size of these devices allows for their easy integration into other systems. Various applications integrating them into conventional bioanalytical methods such as ELISA are expected, because direct measurement of electrical signals does not require separate labels; meanwhile, research has been undertaken to overcome limitations in biosensor performance, considering factors such as the isoelectric point (pI) value, changes in the biomaterials' pH levels, and the Debye screening effect—an effect where the measured electric current values (I_d) vary because the device detection region changes with the ion concentration in the buffer solution [16, 20, 26, 57]. Moreover, some research has reported a fall-of-potential effect caused by electric double layer (EDL), the result of chemisorption on the device's surface, when using commonly available Pt electrodes, on unstable electric current measurement in the FET device interface and electrolyte[16, 49, 58, 59].

The effect of charge screening acts to minimize the total nanostructure volume gated by surface charges, thus reducing device sensitivity; strategies to increase screening length are therefore expected to improve device sensitivity. Maximum device sensitivity may be obtained in situations where the effective screening length is much larger than the nanowire radius. Improved device sensitivity can thus be obtained through careful design and optimization of the several device parameters influencing the effective screening length.

2.2 NanoFETs as biosensors

2.2.1 Operating principles of the nanoFET

The nanoFET operates by injecting liquid state target biomaterial on the surface of sensor. Bioparticles in the water solution will produce electric signals, through immune response or adsorption to the gate electrode between source and drain in Figure 5. As shown in Figure 6, negative charge is adsorbed onto p-type device by biomaterials, and consequently, a channel is created and conductance increases. However, in a solution-based environment, the electric field will not be affected only by signals from the target biomaterials, but also by other complex phenomena as well. It should be noted that FET motions in a solution environment will involve all these phenomena, including noise signals, in a complex way.

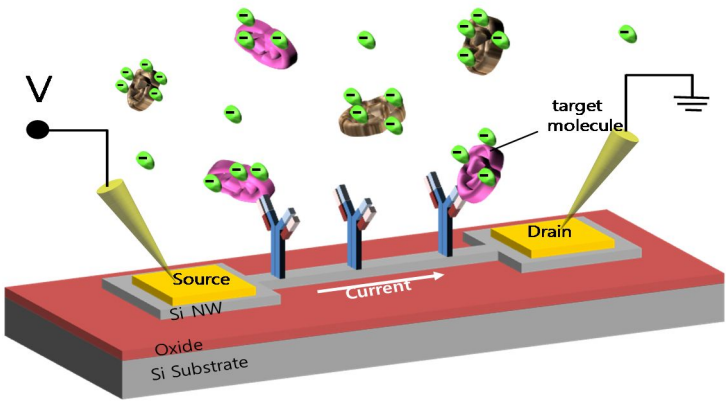

Figure 5. Schematic view of nanoFET sensor operating principle.

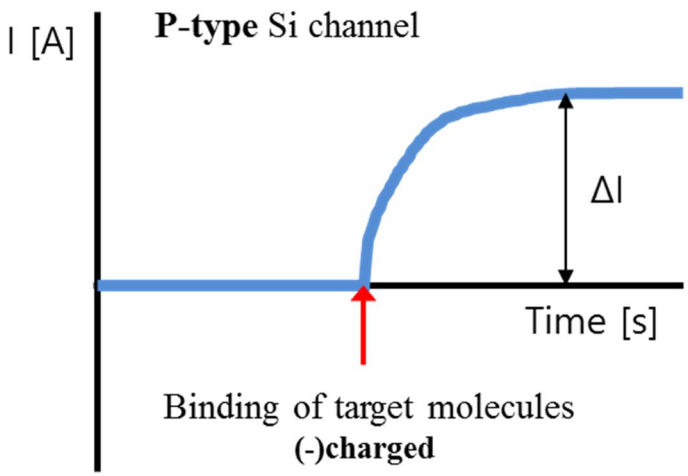

Figure 6. Channel conductivity of a p-type nanoFET device.

2.2.2 NanoFET limitations

A nanoFET device operates on the principle of chemical gating, varying the field-effect through the adsorption of charged particles on the top surface of the gate of a nanochannel. This adsorption process and, hence, the presence of the target material can be detected by measuring the nanochannel conductance variation. This simple detection scheme has the advantage of allowing both easy application and real-time detection, due to the label-free direct detection of the target molecules' charges (through direct measurement of the field-effect-induced channel conductance changes). Many biosensor application research studies have addressed the development of nanoFET-based methods to detect charged particles, such as proteins, DNA, and biomolecules used for disease-related biomarkers, by induced adsorption on their gate surfaces. A field-effect can also be induced on a nanochannel through protonation/deprotonation occurring on the gate oxide film surface, a phenomenon that can be used for detecting pH changes in solutions. Other studies conducted so far involve pH measurement sensors using a nanoFET-based principle: biosensors based on the enzyme-mediated pH detection principle, and pH sensors applicable to DNA sequencing. Many studies on biosensors are focused on quantitative detection of the target biomolecules using the principle of antigen-antibody

reaction, specific to the immune response of biomolecules having an electrical charge or specific intermolecular interaction-induced binding [19].

Concentration of the buffer ions (Debye screening effect)

As described above, Nano wire-FET and nanobiosensors operate similarly to conventional chemical FETs (chemFETs), sensing the presence of bound species by their intrinsic charge [27, 50, 60]. During the conjugation of specific receptor molecules for example ssDNA, antibodies, biotin, and etc and nanostructure surface sensing specific ligands, those specific ligands are eliminated from the surface of sensor with the resolution of the receptor's length, normally between 1 to 10 nm. Recognizing the screening of molecular charge affected by ions that dissolved is the key for analyzing the device output after dissolving the receptors into the solution. It is called the Debye screening effect [19-21, 61-63] . The charge of solution-based molecules and biomaterials is screened by dissolved ions in the solution: electrostatic interactions will make positive ions to encapsulate the negatively charged biomaterial for instance streptavidin. Forasmuch as the ion cloud with positively charged screen out the DNA's internal negative charge beyond the Debye length (λ_D), Coulomb interactions would

clearly have no effect and would only to make neutral charge region seeing from the exterior. Therefore, the molecular charge will be efficiently blinded by dissolved ion at the distance above λ_D. Thus, at distances beyond λ_D, the molecular charge is effectively screened by the dissolved ions. Debye length for aqueous solution at room temperature is given by

$$\text{Debye length}\,(\lambda_D) = \frac{1}{\sqrt{4\pi l_B \sum_i \rho_i z_i^2}} \qquad (1)$$

where l_B is the Bjerrum length (0.7 nm), $\sum i$ is the sum over all ion species, and ρ_i and z_i are the density (6.02×10^{20} cm^{-3}) and valence of ion species i, respectively. That is, the potential shows negative exponential relation with distance; moreover, the Debye length set up the scale of length while potential approaches zero [21].

From (1), the Debye length is 9.1 nm for an ion concentration of 1 mM, 3.6 nm for the 10 mM case, and 0.3 nm for a NaCl concentration of 100 mM. The Debye length in a biosolution of high ion concentration is therefore below 1 nm, which is much less than the length of the protein antibodies; the protein's electric charge has, thus, no electric field-effect on the nanoFET. For a comparative experiment, the ion concentration reaction

were measured in a nanoFET whose streptavidin is not fixed, and only the biotin functional groups have been processed. The nanoFET onto which the protein's charge was adsorbed was different from the nanoFET onto which only the biotin was introduced; when only the ion concentration was varied (with the pH level maintained at 7), the measured resistance of the nanoFET was lower. This result was expected: the resistance decrease was due to the fact that additional holes were induced in the p-type channel due to the field-effect of negatively charged proteins. On the other hand, in the comparative experiment, the change in resistance of the nanoFET onto which only the biotin was introduced was negligible, for the same ion concentration (see Figure 7).

In this experiment, this study used two different buffer concentrations of phosphate buffered saline (PBS) buffer: 1 mM PBS, and 100 mM PBS. Reducing the buffer concentration increases the Debye length, which leads to an increase in the sensing area. These dilutions were made relative to 1X PBS, which contains 150 mM NaCl, 3 mM KCl, and 10 mM phosphate salts. These values show that, for functionalized nanoFET measurements (those relying on a receptor-ligand binding event), careful consideration must be given to the buffer ionic strength, so as not to screen the ligand. Debye screening constitutes an important design consideration for label-free nanoFET detection, to optimize buffer concentrations when using bioFET

sensors.

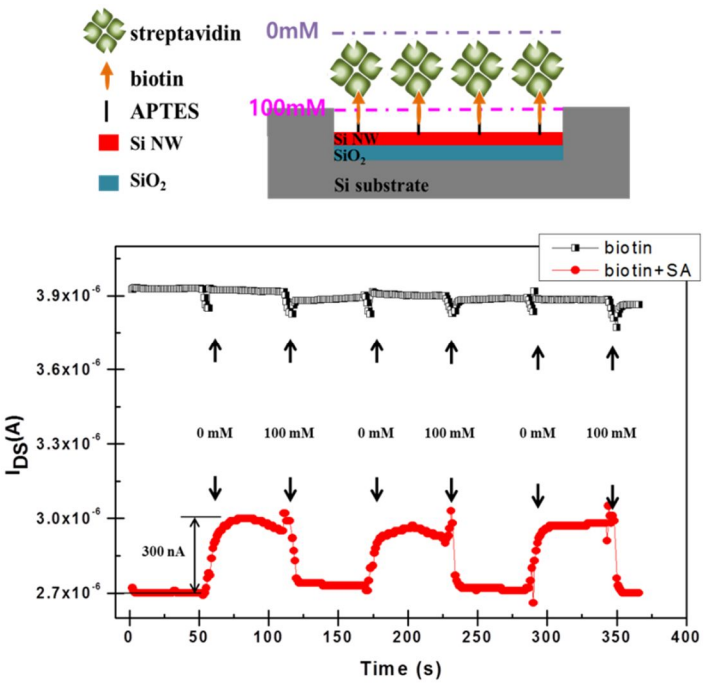

Figure 7. Debye screening length and current variation corresponding to different NaCl concentrations at a given pH value.

Solution potential (According to the reference electrode)

This study next discuss the noise that can be generated by the solution's electric potential. This electric potential affects the channel's electric field; the potential of the reference electrode must therefore be kept stable. It was

verified that the half-cell potential between the solution and the reference electrode varied with the type of reference electrode. Thus, when the solution is being replaced, the potential between the reference electrode and the solution wavers unstably, which, in turn, affects the potential between the solution and the channel, as shown in Figure 8. Using both the Ag/AgCl and Pt as reference electrodes, the difference was examined in spurious signals generated by the change in potential of the solution [17].

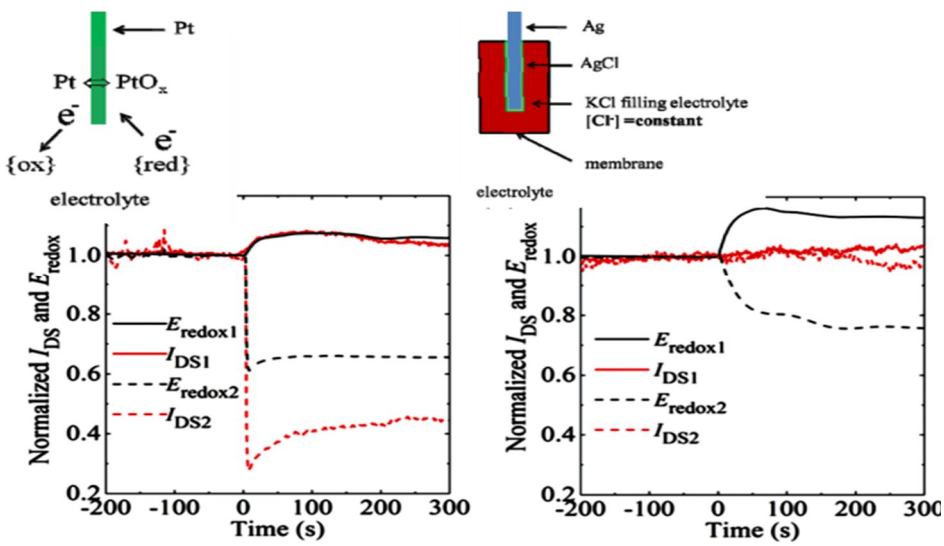

Figure 8. Solution potential effects for different reference electrodes.

Small sensor surface area (diffusion issues)

This study now address the problem created by relatively low concentrations of detected biomaterial per detecting surface area of the nanoFET. Another difficulty lies in the actual adsorption of the protein's charge on the nanoFET channel's surface. Reference [48] reported that the nanoFET sensor detected proteins at 1 fg/mL concentration. Let us convert this result to the number of molecules in the solution, using the molecular weight of prostate-specific antigen (PSA) (33 kDa), which is used as marker for prostate cancer. The surface area of a general nanoFET device exposed to 10 μL of the sample solution has a length of about 10 μm and a line width of 0.1 μm.

Table 2. Parameters to calculate the number of molecules in the volume of Figure 9

Item	Calculation
Mass of PSA in the box.	10^{-9} ng = 10^{-18} g
Molecular weight of PSA.	33000 g/mol
Moles of PSA in the box.	3.03×10^{-23} mol = 10^{-18} / 33000
Number of PSA molecules in the box	18.24 = $6.02 \times 10^{23} \cdot 3.03 \times 10^{-23}$

Using the parameters in Table 2, converting 1 ng/mL to a number of molecules per unit volume results in 18×10^7 molecules/10 μL, which is about 200 million protein molecules per 10 μL of solution. Also, the concentrations of 1 pg/mL and 1 fg/mL are converted to 18×10^4 molecules and 180 molecules in 10 μL of solution, respectively. Thess results can see that for a PSA concentration of 1 fg/mL and a nanoFET surface area of 10 μm × 10 μm × 10 μm, there are about 200 antigens in the vicinity of the sensor's surface. In other words, in 10 μL of the solution, there are roughly 200 million molecules for a 1 ng/mL concentration, 200 thousand molecules for a 1 pg/mL, and 200 molecules for 1 fg/mL concentration. The

interpretation of this experimental result alone suggests that adsorption occurs immediately after the solution is injected, regardless of its concentration [48].

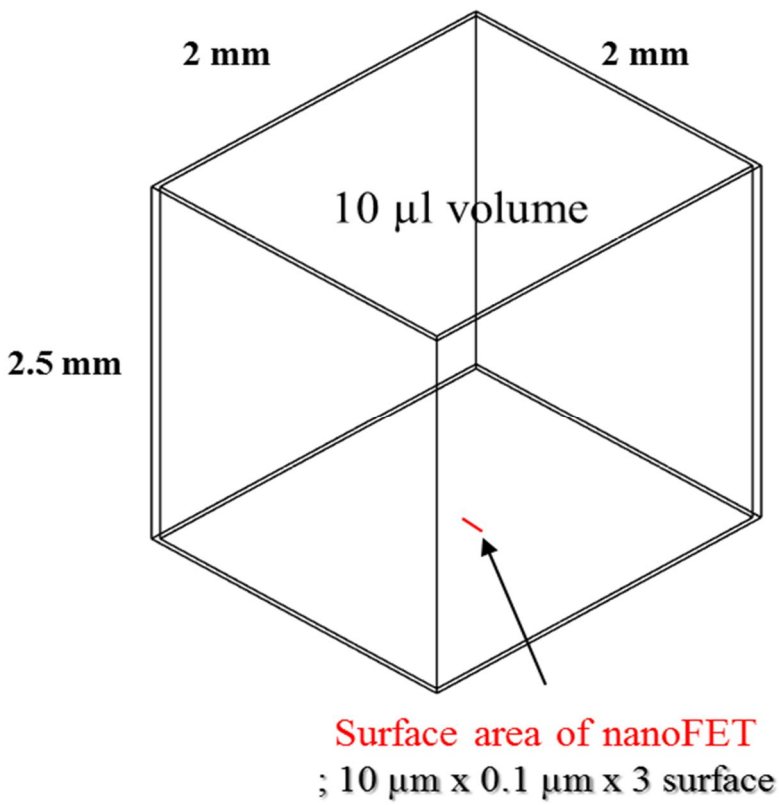

Figure 9. Illustration of a 10 µL volume of PSA solution and the surface area of the nanoFET.

As can be seen in Figure 9, detection of the target proteins requires an amount of time (proportional to the volume), sufficient for the immune

reaction, or for it to be adsorbed to the sensor's surface. Applying this reasoning to PSA detection with an actual nanoFET results in a detection signal suggesting that the reaction happens gradually. However, most experimental results of nanoFET protein detection deal with relatively short reaction times of tens of seconds, as shown in Figure 10. These results can be thought of as being the momentary instability of the sample solution's potential during injection, rather than being the target material's signal.

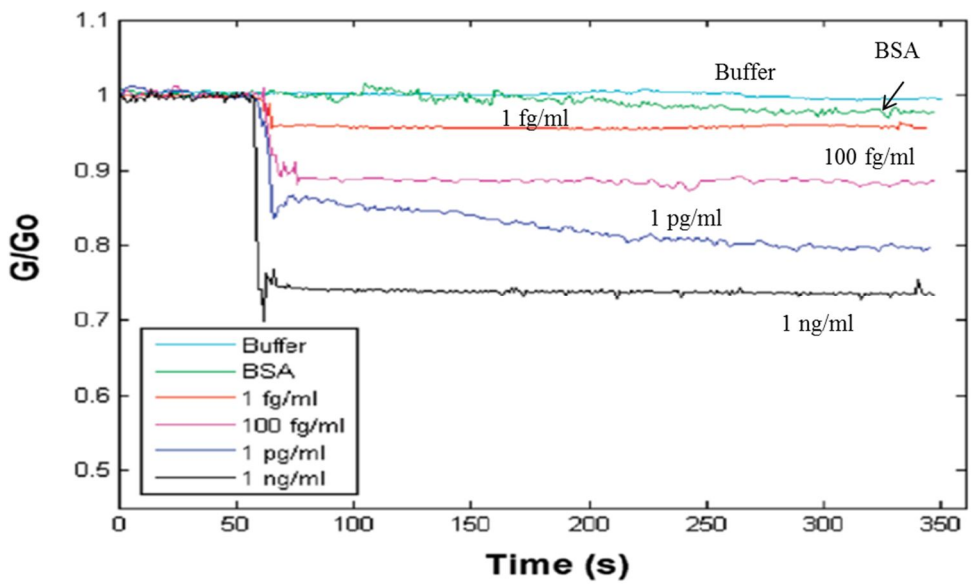

Figure 10. An experiment not spanning the time required for a response to the target substance on the nanochannels.

2.3 Summary

When using nanoFETs as biosensors, this study must be take into account the fact that several phenomena are intervening in the measurements, in complex ways; this includes the Debye screening effect, noise signals originated by the solution's potential, and the characteristics of the reaction on the surface of nanoFET device due to diffusion. It is very difficult to measure the change in the nanochannel's conductivity due to chemical gating using the sample solution.

In this study, an experiment was conducted on the chemical gating operating principle of the nanoFET sensor, using airborne anions. This study also proposed the novel application of detecting the air concentration of anions using nanoFETs. In air, only the adsorption of charged particles is observed, without the noise effects discussed earlier. A sensible interpretation of these effects will allow for a clearer understanding of the nanoFET sensor, leading to better control of the experiment in a solution environment.

Chapter3.
Design and Fabrication of NanoFETs

3.1 Introduction

The initial study of nanowires was focused on synthesis; a fair amount of research on their basic properties has therefore been conducted, as seen in Figure 11. However, despite their superior electrical properties, the use of nanowires as components has been limited by the difficulty in handling them. In particular, the bottom-up style of nanocomponent development presents technological difficulties to selective arrangement in large-area nanostructures, which have been limiting its mass production in several ways [51, 60]. Other concrete problems, including not only mass production but also securing reproducibility and increasing reliability, have remained unsolved [51, 52].

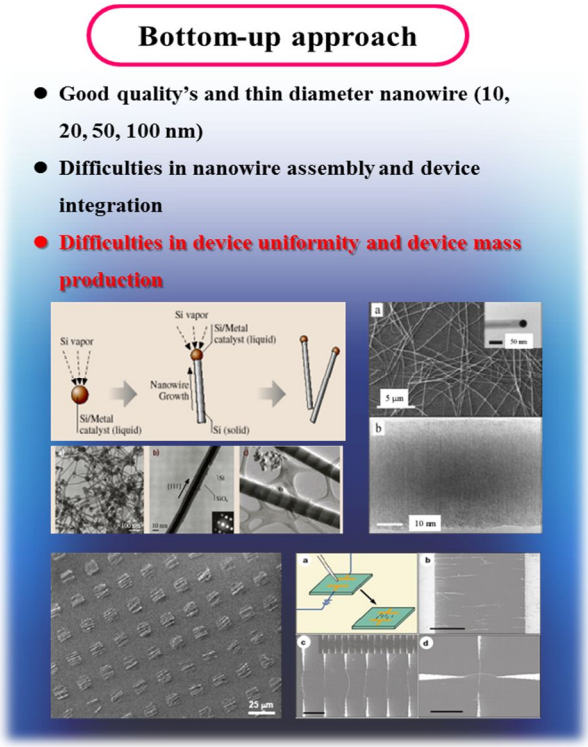

Figure 11. Research in nano structures synthesis and properties

The recent manufacturing process simplification using SOI wafers allows for mass production and presents some advantages. In this study, this method was proposed for mass production of nanoFET devices to be used as biosensors, and the MEMS process to facilitate fabrication, as shown in Figure 12 [15, 27]. This method was designed to evaluate its performance also. To fully evaluate the strengths of the SOI wafer-based process, an experiment was performed, whose goal was to develop a nanoFET platform suitable for commercialization, and evaluate its performance. In addition, to

reduce the external noise generated during injection of the liquid specimen into the nanoFET device, a biosensor platform was developed, by designing a printed circuit board (PCB) and an interface for measurement. Many research studies on nanoFET biosensors are being published, using a top-down approach to achieve these same goals [8, 15, 27, 35, 53]. The top-down method uses the same process technologies widely used in CMOS silicon semiconductors, to fabricate a nanoscale FET and apply it to a biosensor; therefore, it has the great advantage of possessing the potential to be mass produced and commercialized. In the United States, Professor Reed's research team, at Yale University, has developed a FET biosensor with a silicon nanochannel formed by photolithography and etching, based on a silicon-on-insulator (SOI) wafer. The same team also evaluated the performance of this biosensor for several proteins—including the T-cell and streptavidin—and various CMOS processes, and has reported that it is possible to analyze traces of 100 fM in real time [28].

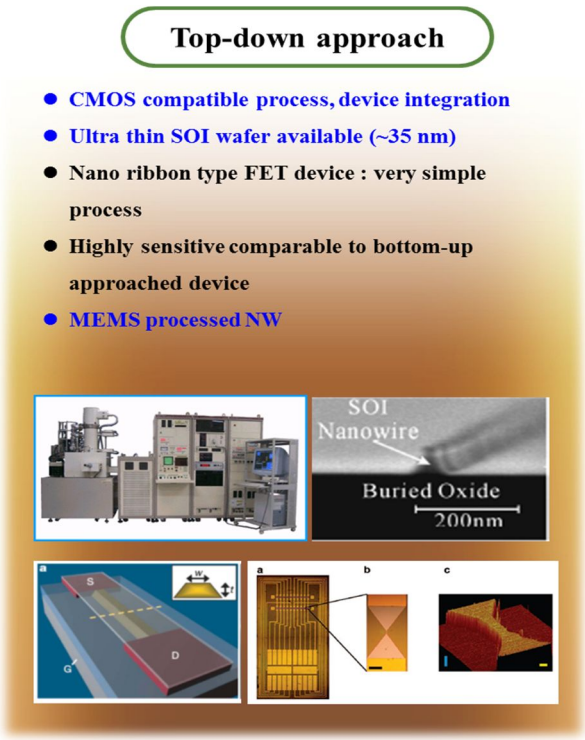

Figure 12. Research on manufacturing methods suitable for mass production.

3.2 Design

In the previous chapter, the several error sources present was discussed when using nanoFETs as biosensors with liquid samples. This study saw that one of these sources was the low probability of specimen's reaction in the nanochannel, due to the small size of the device. The nanoFETs designed in this study have channels with line widths—which determine the range of detection—larger than that of nanoFETs designed with the bottom-up method, and can be fabricated by a relatively simple MEMS process, using an SOI wafer. The nanoFETs were designed to have channel lengths of 5 μm, and line widths of 1 μm and 0.4 μm. Specifically, three components were designed: the first one with a channel length of 5 μm and a line width of 1 μm, the second with a length of 5 μm and a line width of 0.4 μm. The components are labeled L5W1, L5W0.4, and L2W1, respectively. Figure 13 presents the cross sectional structure of the proposed nanoFETs.

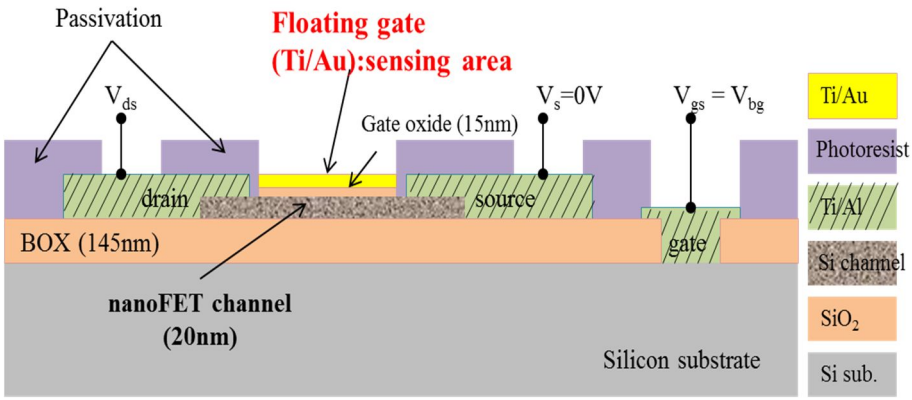

Figure 13. Schematic of nanoFET (cross-sectioanal view).

Figure 14 shows the arrangement of 10 nanoFETs produced as an array on a single chip. This array form was used to facilitate electrical measurements by wiring it to a PCB, and producing a separate measurement block. In addition, biosensors generally use a liquid specimen; a reference electrode is hence used to control the solution's potential. In particular, to reduce the noise signals generated during the injection of solutions with different pH levels, and to fix the position of the reference electrode, a separate manufactured block was used, in addition to the nanoFET's PCB.

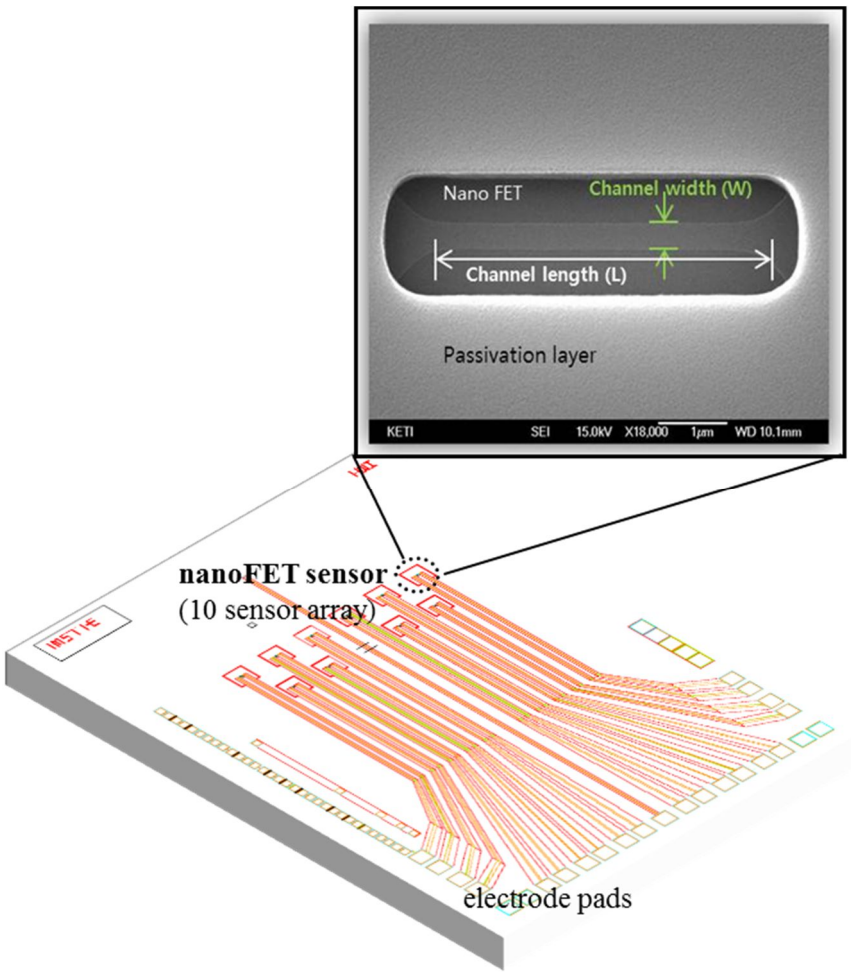

Figure 14. NanoFET array on the chip (schematic view), and FESEM image of nano channel and sensor surface (top illustration).

3.3 Fabrication

The proposed nanoFET sensor was produced using general micromachining technology. This study attempted to simplify the process and avoid wet etching, which is a relatively intricate process, by using thin SOI wafers. The fabrication process was thus simplified (when compared with the existing top-down fabrication processes) by not using wet etching [7]. The handle silicon substrate is used as a universal bottom gate electrode (with back-gate voltage V_{bg}). Each nanoFET has a 20 nm thick silicon channel, and a 15 nm thick SiO_2 gate oxide layer, for negative ion adsorption. The buried oxide (BOX) layer and handle silicon substrate have 145 nm and 500 μm in thickness, respectively. The passivation layer is a 1 μm photoresist (PR). The nanoFET channel is placed on the substrate (bottom gate electrode) and a floating gate is formed atop the gate oxide film deposited on the nanoFET channel. The thicknesses of the nanochannel, gate oxide, floating gate electrode (Ti/Au), and BOX are 20, 15, 10/100, and 145 nm, respectively. Figure 15 shows the nanoFET layers without metallization.

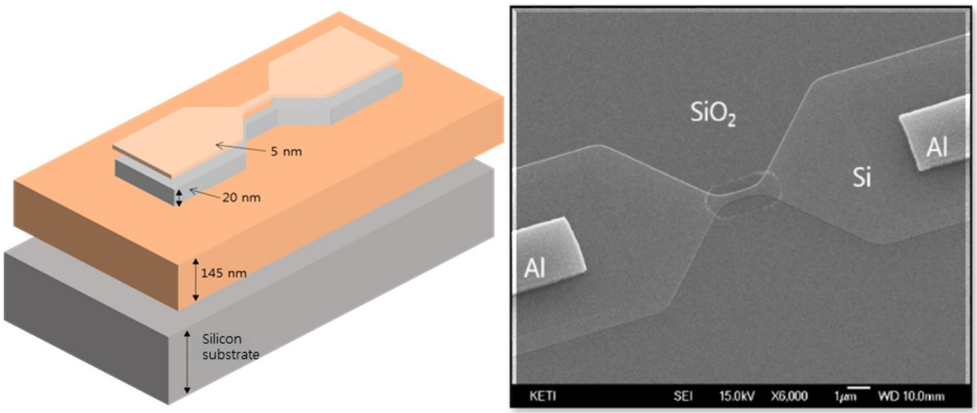

Figure 15. Illustration of the Si substrate, BOX oxide, nanochannel (nanoribbon), and gate oxide layers.

To compare operation characteristics, nanoFET devices with a floating gate structure was fabricated, by forming an additional gate electrode on the nanoFET channel structure. Figure 16 illustrates the production process of the nanoFET device with the additional floating gate electrode. Figure 16(a) shows the inicial step of the fabrication process. Starting with a thin SOI substrate (SOI tech, France), the silicon nanochannel is thinned by thermal oxidation to a thickness of 20 nm, from the initial 70 nm thick top layer. The silicon nanochannel thickness uniformity obtained with the thermal oxidation thinning process was within 6% of the target 20 nm thickness, in an 8-inch wafer. The 8-inch SOI silicon process was performed with the facilities of the National Institute for Nanomaterals Technology (NINT, Korea); the boron implantation process was performed in the National Nanofab Center (NNFC, Korea). The SOI wafer-based silicon film on

which the nanochannel is to be formed undergoes both thinning (through thermal oxidation) and patterning. The BOX is patterned, to ensure contact and interconnection with the bottom substrate electrode. Contact areas and channel doping are achieved by implantation. Boron (B^+) implantation for contact doping was done at a dose of 5E15 and an energy of 3 keV, and B^+ was implanted (dose of 1E13, energy of 3 keV) on the wafer front side, for channel doping. After the contact doping implantation process, rapid thermal oxidation (RTO) followed, for implantation annealing and gate oxide formation. Rapid thermal oxidation (RTO) was performed to form a 15 nm gate oxide, followed by a lift-off process to depose a Ti/Al(10/200 nm) electrode for source/drain contacts and bottom gate interconnection. A floating gate electrode was then formed with Ti/Au(10/100 nm), using a lift-off process. Finally, PR patterning was performed, so that only the sensing area remained exposed. All parts excluding the area for target substance detection (gate electrode), the source, and the drain were coated using PR, passivated to allow detection of the electrical signals of the liquid sample. The fabricated nanoFET devices were designed to measure the change in conductivity and, thus, detect several liquid samples of different pH levels and airborne anions.

When used as biosensors, the nanoFET devices comprise a ribbon with a nanoscale thickness using SOI substrate or a one-dimensional nanowire-

shaped fieldeffect channel, a substrate electrode for channel biasing control, a gate oxide film deposited atop the nanochannel (the sensing surface), and a receptor formed on it with a chemical functional group or biomaterial enabled to detect specific biomolecules through chemical surface treatment. The nanoribbon-shaped Si structure's surface, which is the part that detects the sample, was processed with O_2 plasma, reforming it to OH-. Additionally, 3-Aminopropyltriethoxysilane (APTES, 2% v/v in ethanol, 99% anhydrous) was processed, using a mixer for an hour at room temperature, to introduce an amino group ($-NH_2$). The silane that did not react after the amino group was introduced was cleaned, using ethanol and DI water. The device whose surface was reformed was kept dry until use. It was then introduced to the terminal of the surface reformed by APTES, to detect the change in the concentration of hydrogen ions, according to the change in pH level.

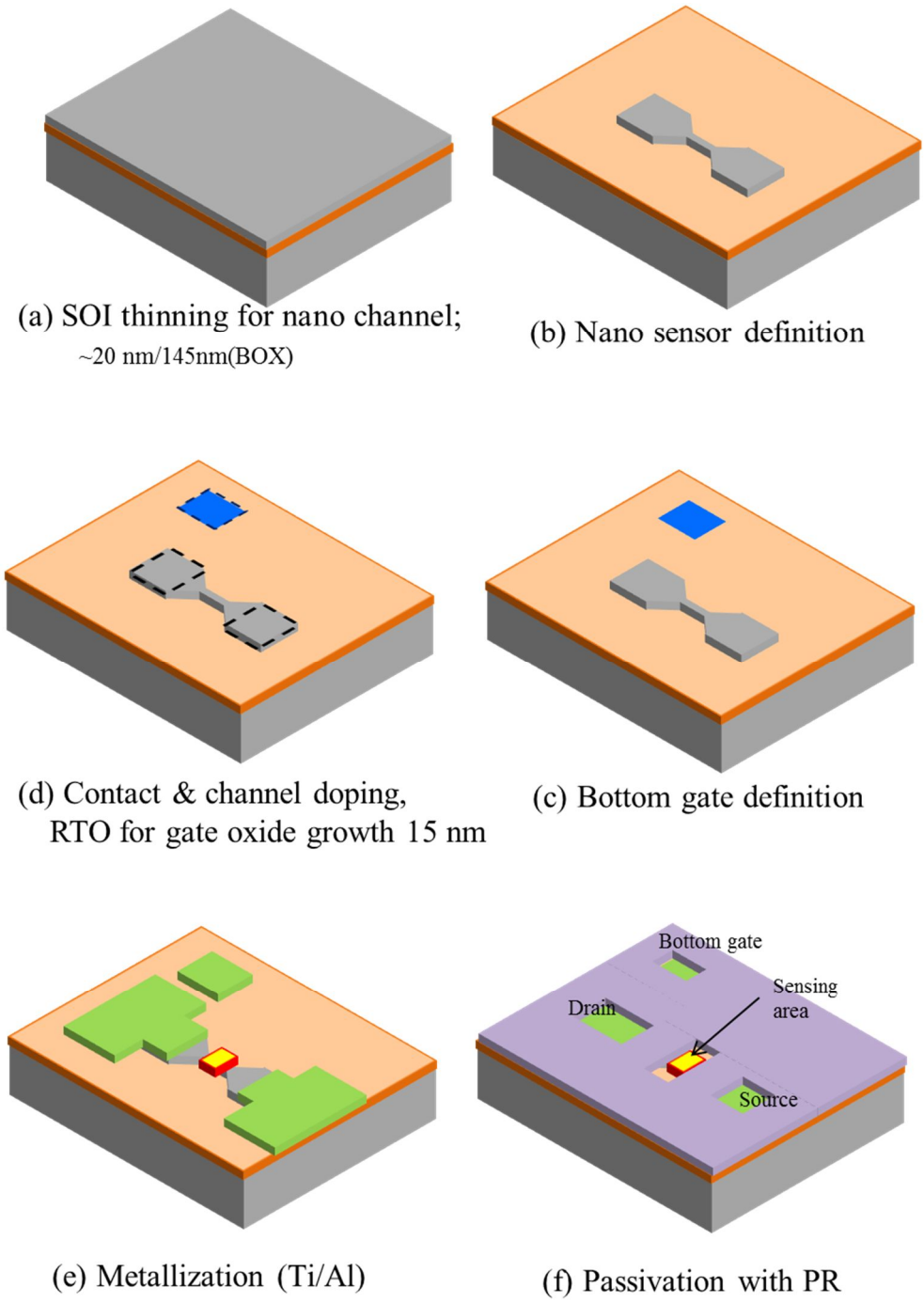

Figure 16. Fabrication process of the nanoFET sensor.

For comparative testing, we fabricated two types of nanoFET sensors; one, with a nanoFET channel and gate oxide film, and the other with an additional floating gate electrode. Figure 17 shows the SEM images of the fabricated nanoFET sensors. We analyzed the operation mechanism of these devices by assessing the channel conductance variations provoked by the field-effect of airborne ions, using both types of nanoFET sensors: the nanoFET sensor with gate oxide, and no top-gate electrode, and the nanoFET device with a floating gate structure atop the gate oxide. Figure 17(a) shows the nanoFET structure with gate oxide deposition without a top-gate electrode, and Figure 17(b) shows the nanoFET with an additional floating gate electrode formed atop the gate oxide film. The entire surface was passivated with PR, except for the sensing area.

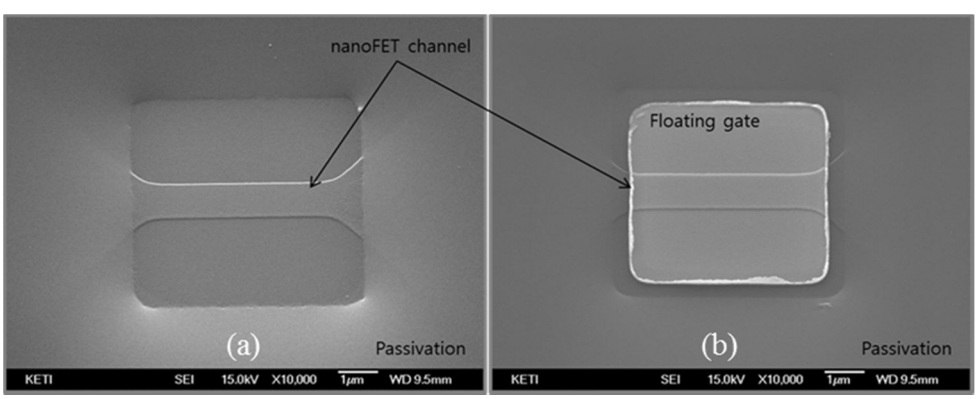

Figure 17. SEM pictures of fabricated nanoFET sensors. (a) NanoFET sensor without floating gate. (b) NanoFET sensor with floating gate structure.

3.4 Summary

The proposed nanoFET devices were produced on a SOI wafer, to increase productivity by reducing the complexity of the fabrication process. The nanoFET was produced by general MEMS fabrication processes, such as dry etch and photolithography. Ten independent nanoFETs were designed in one chip, as an array to be used for multi-sensing and repeated experiments. The proposed nanoFET array was fixed on the PCB. The thicknesses of the nanochannel, gate oxide, floating gate electrode (Ti/Au), and BOX are 20, 15, 10/100, and 145 nm, respectively. The floating gate metal electrode deposited on the gate oxide is also used to widen the sensing area. Except for the sensing area, the surface was passivated with PR to provide electrical isolation between the source and drain electrodes.

Chapter 4.
Detection of Anion in the Air

4.1 Introduction

In the case of a biosensor operating inside a solution and using the reaction of protein or biomolecules, the operating environment of the solution and the specific bindings between antigen and antibody or target and receptor cause adsorption at specific distances, which may differ among different cases However, they can all be expected to show similar behavior, because in all cases a chemical gating process is taking place: the change in conductivity due to the field-effect caused by the adsorbed charge. In all cases, the slope of the drain-source current (I_{ds}) will allow us to observe the adsorption of the sample to be detected. I_{ds} will show a low rate of change for low concentrations and vice versa, while approaching the saturation value of I_{ds}. This rate of change (i.e., the slope of I_{ds}) will appear as a function of the speed of adsorption due to differences in the target objects. In addition, there will be small differences in saturated I_{ds} among concentrations, but at low concentrations, with low slopes, the amount of adsorption will increase; we can thus verify that the FET sensor is operating correctly if the target sample's concentration is being reflected by an appropriate change in the observed signal. Different I_{ds} slopes are to be

expected for the adsorption of protein charges in a solution and the absorption of airborne ions, because the target molecules/anions velocity and speeds of adsorption are different, and will cause differences in the I_{ds} slope, but the change tendencies are expected to be very similar.

In this study, we tested the feasibility of using a nanoFET sensor to detect anions in the air. We experimentally demonstrated that the concentration of anions in the air can be detected by the conductance change of the field-effect channel, due to the adsorption of charged particles on the nanoFET gate sensor surface. From the anion detection experiments in the air, the characteristics of chemical gating—the operating mechanism of the nanoFET biosensor—were evaluated. Since the pH, solution potential, and ionic strength in the buffer have minimal variations in air, it was easy to measure the electric field-effect caused by the adsorption of charged particles, and characterize the mechanisms of the field-effect-transistor. In this study, we demonstrated the operating mechanism of chemical gating, by measuring and analyzing both the conductance change and response characteristics of the nano-field-effect channel, using various anionic concentrations in the air.

4.2. Measurement results

Figure 18 shows the experimental set-up used to detect negative ions in air using the developed nanoFET sensor. Airborne negative ions are generated and spread out by a commercial ionizer. Anionic concentrations at the sensor location are adjusted by controlling the distance between the ion generator and the nanoFET sensor; this distance varies from 10 cm to 70 cm, at 10 cm intervals. A shutter is used in front of the sensor, to expose or block the anions spreading out from the ion generator. To perform real-time measurements, the shutter opens only at the intended times. The ion generator used for the experiment was a commercially available air ionizer (Dr. USB, IMH Co. Korea), which consists of a small blowing fan and tip electrodes for air ionization based on the arc discharge method [64]. Figure 18 depicts the experimental scheme used to measure and evaluate the properties of the nanoFET sensor for the detection of anions in air. The concentration of negative ions in the air can be modulated by changing the distance between the sensor device and the ion generator. A fan in the generator allows the generated negative ions to spread and reach the nanoFET sensor [57]. Experimental results for the distance control are reported in KMEMS2014 and for information on quantitative detection of negative ions in air it was released from KMEMS2015.

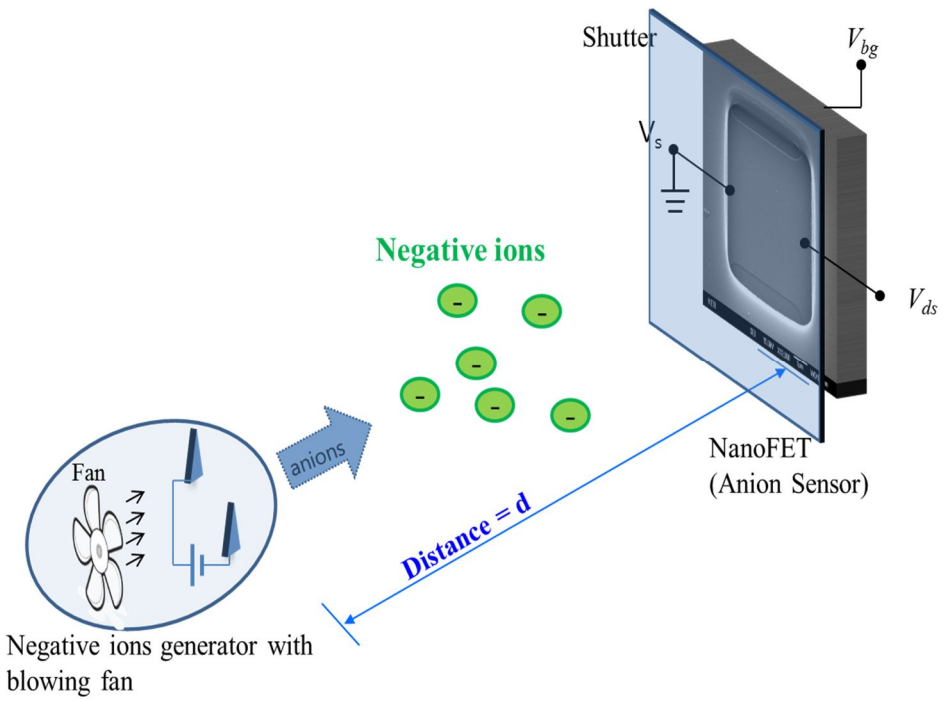

Figure 18. Experimental setup to detect negative ions in air using the developed nanoFET sensor.

4.2.1 Detection of anions in the air

Figure 19 shows the current-voltage (I_{ds}–V_{bg}) characteristics of the developed nanoFET device, obtained by varying V_{bg} from negative to positive values. We compared the initial fabricated state (rectangular dotted line), the charged state due to negative ions exposure (X-labeled dotted line), and the steady state reached after some time has passed with the ionizer off (triangular dotted line).

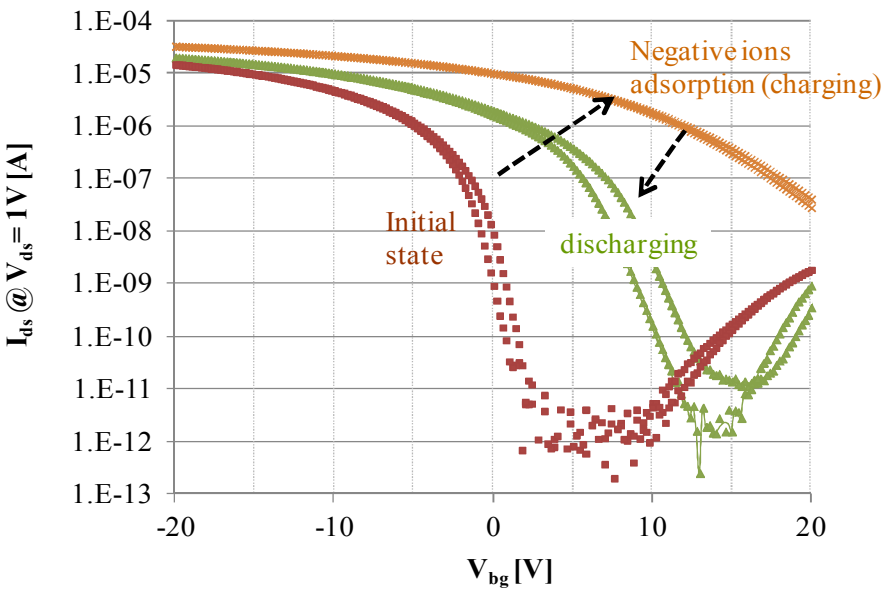

Figure 19. *I-V* characteristics measurement for negative ions exposure.

The p-type FET I_{ds}– V_{bg} characteristics shows high performance properties: when the back-gate modulation varies from –20 V to +20 V with constant V_{ds} = 1 V, an I_{on}/I_{off} ratio greater than 10^7 and a transconductance (g_m) of 1.05 μS are obtained. When the channel surface of the nanoFET device was charged by the airborne negative ions, the I-V curve moved to the right-upper side, as shown by the X-labeled dotted line in the referred I_{ds} – V_{bg} graph. The shift corresponds to the quantity of negative charges on the channel surface. It is therefore reasonable to conclude that negative ions may be adsorbed on the surface of the FET channel when the negative ion concentration in air increases in the vicinity of the nanoFET sensor, during operation of the air ionizer. After the ion generator was turned off, the I-V curve recovered, over time, towards the initial state, as shown by the triangular dotted line. This is most likely due a reduction of adsorbed charge caused by charge leakage. However, it did not recover completely to the initial state.

Figure 20 shows the real-time nanoFET response to negative ions in air. The drain-source current (I_{ds}) at constant drain-source voltage (V_{ds} = 0.1 V) increases according to the imposed back-gate voltage (V_{bg}) modulation from 0 V to –15 V, in –5 V increments, which represents typical p-type channel FET properties. The ionizer was turned on at t = 200 sec, with V_{bg} = 0 V. I_{ds} increased gradually, and finally became saturated, as shown in Figure 20.

This proved the existence of negative ion adsorption or negative charge accumulation on the channel surface. Furthermore, this result shows that the nanoFET could detect negative ions in air. The sensitivity of the device, $\Delta I/I_o$, reaches values above 700. The I_{ds} increase rate with time, which is the slope of I_{ds} in the graph, has a maximum of approximately 80 nS/s.

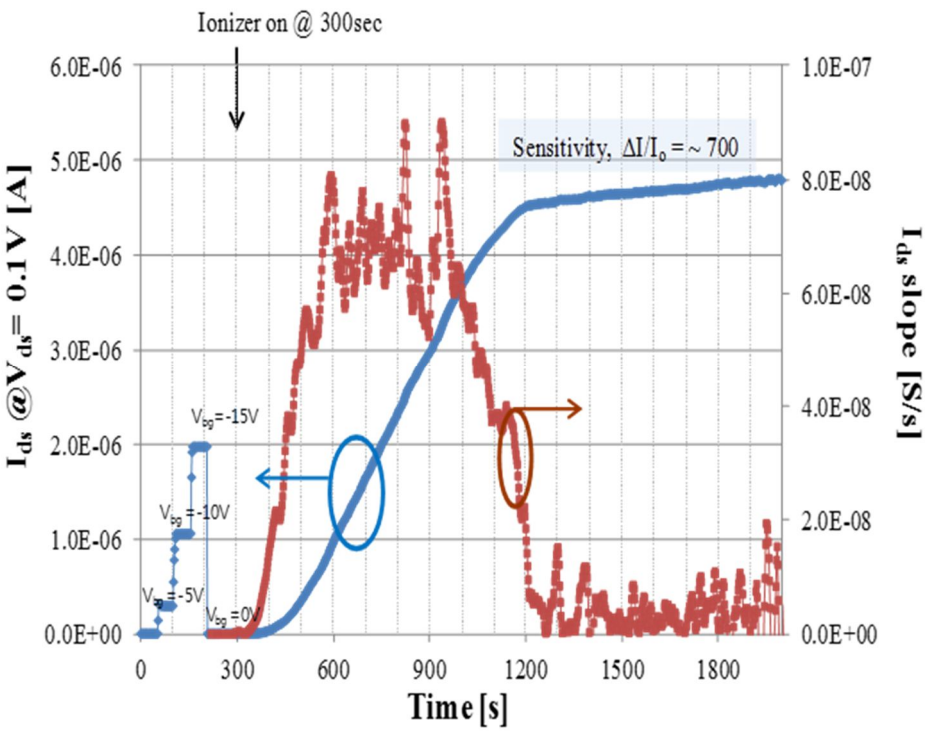

Figure 20. Real-time detection of airborne negative ions using a nanoFET sensor.

To numerically calculate the number of negative charges adsorbed on the sensing area, a metal-oxide-semiconductor (MOS) capacitance based calculation is used. We may assume that the silicon nanochannel confines with two parallel plate MOS capacitors on the channel top and bottom; the top capacitor comprises of gate oxide and sensing area, and the bottom capacitor comprises the BOX insulator and the back-gate silicon substrate. If an electric field is applied to the silicon nanochannel through both top and bottom equivalent MOS capacitors, we can calculate the charge using the following equation:

$$Q_{bg}=C_{box}V_{bg} \qquad (2)$$

In (2), C_{box} is the capacitance of the BOX layer capacitor, and V_{bg} is the applied back-gate voltage. If the nanochannel conductance level induced by the applied back-gate voltage equals that of the electric field created by the adsorbed charges on the top sensing area of the top capacitor, then the adsorbed charge Q equals Q_{bg}. Therefore, for $C_{box} = 6.1 \times 10^{-15}$ F, $V_2 = V_{bg} =$ 15 V, we obtain $Q = 9.15 \times 10^{-14}$ C, implying the existence of 5.7×10^5

individual charges. The ionizer is known to generate anions with approximately 2×10^6 ea/cm^3 at 5 cm away from the ionizer. The amount of adsorbed charges is proportional to the adsorption coefficient A and ion concentration in air D; hence, the adsorbed charges on the sensing channel are also proportional to D ($Q = \alpha D$). The maximum value for α is 1; therefore, the obtained experimental numerical results are reasonable. The information in this chapter has been reported in Micro and Nano Systems Letters[57].

Real-time measurement

Figure 21 shows the result of measuring the operating characteristics of anions. The p-type FET device maintains the reference level, and at t = 50 s, when anions are adsorbed, the channel's conductance gradually increases until it becomes saturated, as expected. After saturation, the nanochannel's conductivity remains constant, and at t = 300 s, when the cations are adsorbed, conductance decreases. We can understand this behavior as the result of the field-effect due to chemical gating the p-type component. The gradual I_{ds} increase when anions are adsorbed (up to saturation), derives from the very nature of the p-type channel (whose conductance is supported

by positive charges). Figure 21 shows the typical results characterizing nanoFET sensor-based real-time air ion detection devices; a nanoFET sensor without the top-gate electrode was used.

Figure 21 shows the real-time ion detection characteristics of the nanoFET sensor without the top-gate electrode. Under the condition V_{bg} = 0 V (channel turned off), I_{ds} = 0.1 nA, and V_{ds} = 1 V, anions in air were induced to reach the center in the constant ion strength. As anions are adsorbed, I_{ds} gradually increases up to saturation because of the resulting p-type channel reinforcement. NanoFET sensors with floating gate behave present the same behavior.

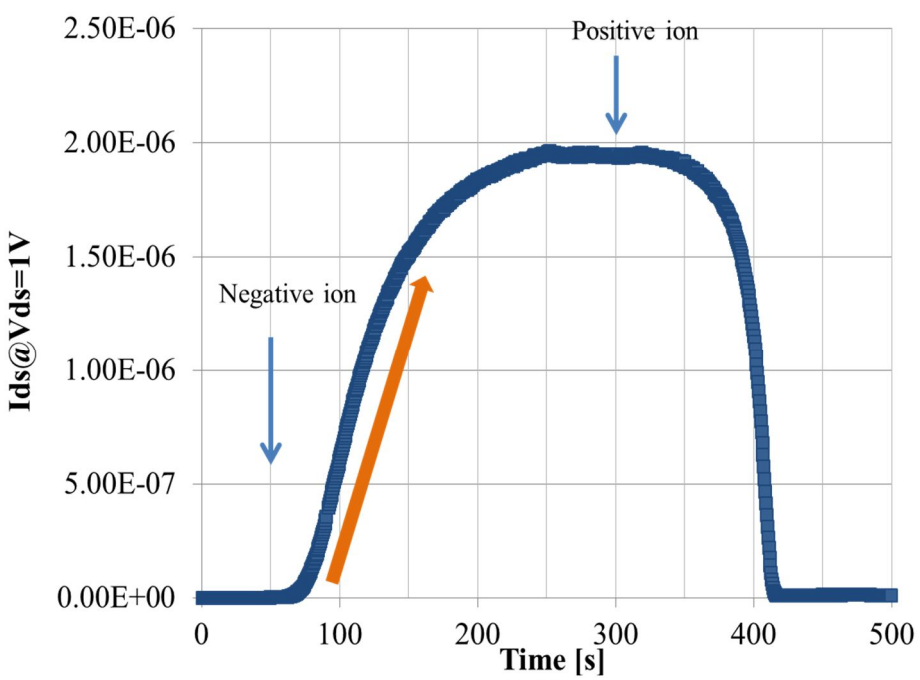

Figure 21. Obtained results of real time anion detection.

Figure 22 compares the real-time anion detection characteristics of sensors with and without the floating gate electrode (top: linear scale; down: log scale). Although the different structures of both sensors can pose difficulties to the direct comparison of their anion detection characteristics (because of the influence of sensor material-dependent anion adsorption coefficient and nanochannel biasing), it was verified that the nanoFET with a floating gate electrode detected anions faster. We assume that this faster I_{ds} detection rate is attributable to the gate electrode structure, because the device without this electrode poses problems, when repeated measurements are to be made with the same device.

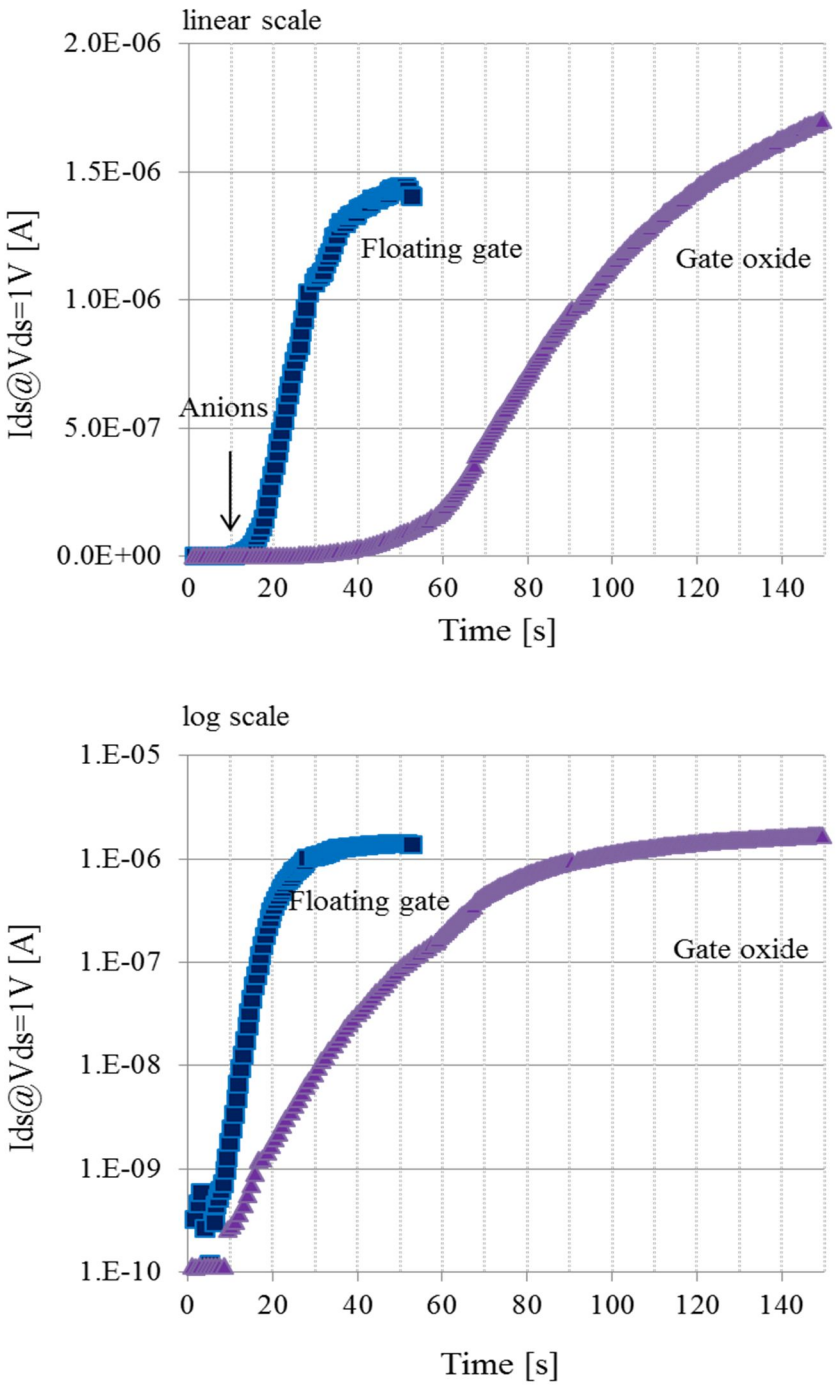

Figure 22. Comparison between devices with and without a floating gate electrode; linear scale (top) and log-scale (down).

I-V characteristics with back-gate modulation

The $I_{ds} - V_{bg}$ characteristics of the nanoFET are shown in Figure 23. The black triangular dotted line represents I_{ds} versus V_{bg} in linear-scale (left y-axis) and the blue circular dotted line shows the same current in log-scale (right y-axis). The red square dotted line represents the transconductance (g_m) of the device. The {1, 2, …, 5} locations in the V_{bg} axis represent the bias voltage values used to evaluate device sensitivity at that particular V_{bg}.

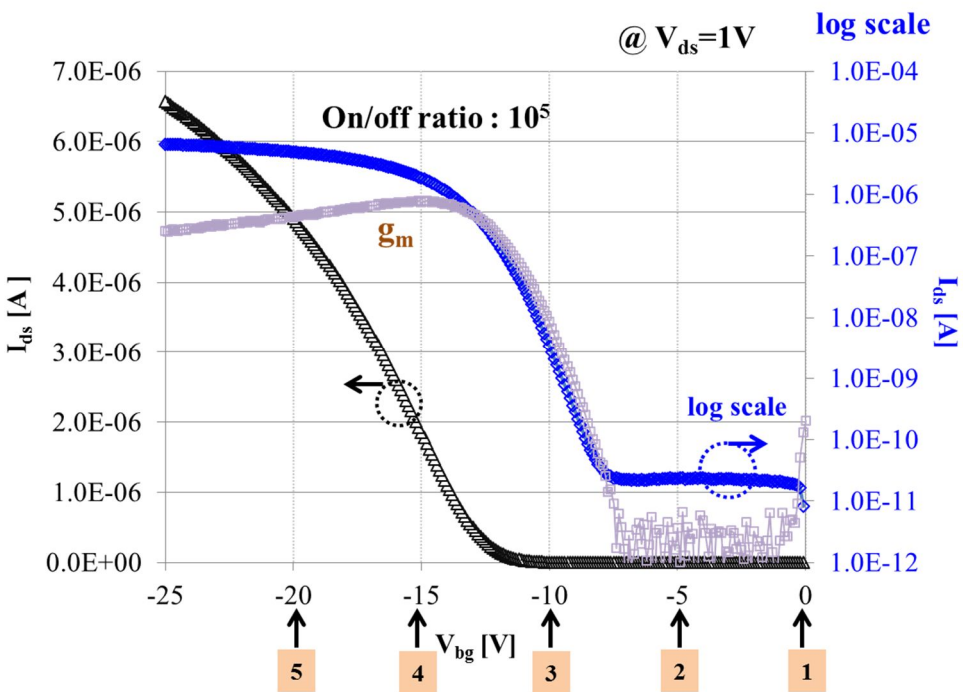

Figure 23. *I-V* characteristics of the nanoFET device for a back-gate voltage (V_{bg}) variation from 0 V to 25 V at a constant V_{ds} of 1 V.

The I_{ds} versus V_{bg} curve was plotted in both linear scale (left *y*-axis) and logarithmic scale (right *y*-axis). The nanoFET behaves as a typical p-type channel device, with a high I_{on}/I_{off} ratio of above 10^5, and a transconductance (g_m) of 790 nS/V at V_{ds} = 1 V. We selected five back-gate bias voltage values of V_{bg} from –20 to 0 V with 5 V intervals, to evaluate the sensitivity of the nanoFET sensor with the channel in those particular conditions. At V_{bg} values of –20 and –15 V, the channel was turned on, in the linear region, and g_m was maximized for V_{bg} = –15 V. At a V_{bg} value of –10 V, the device was in the subthreshold region. At V_{bg} values of –5 and 0 V, the device was in the fully depleted (turn-off) region. We thus experimentally determined the channel conditions under which the sensitivity of the nanoFET sensor was maximized. We compared the sensitivity in five different channel regions of the nanoFET to be determined by the back-gate bias potential as linear, subthreshold, and depleted channel states, respectively, as marked on the *x*-axis in Figure 23.

Quantitative detection of negative ions

As shown in Figure 24, channel conductivity was measured in real time, for a fixed anionic concentration and varying substrate gate bias. The

conductance change was measured twice, for five different back-gate potential regimes, with a constant anionic concentration of approximately 40,000 ea/cc. It was shown therein that I_{ds} gradually increased over time, up to its saturation point. This indicates an accumulation of anions on the sensor surface. Attention should be paid to the delay in I_{ds} change occurring under gate bias conditions 1 and 2, in the depletion region in the turn-off channel. The value of this delay increased under voltage conditions with higher depletion.

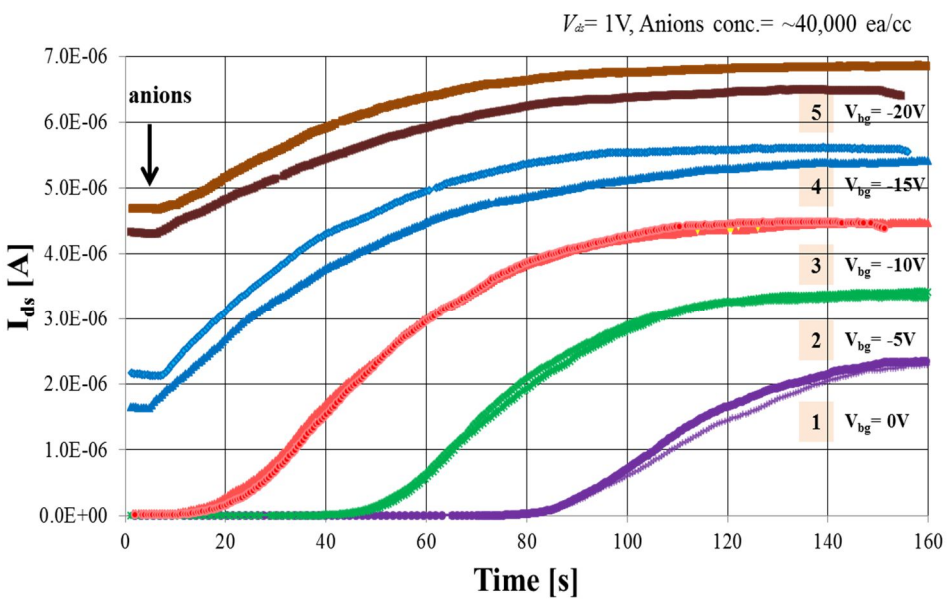

Figure 24. Results for real-time detection of negative ions at the depletion, subthreshold, and linear regions of the nanoFET.

It is interesting to note the increase in I_{ds} induced by hole accumulation, once a sufficient amount of ions accumulates on the sensor surface, and thus, gives rise to the field-effect in the channel. For a sensor that operates by detecting the concentration of the target object (under the assumption that it reacts to the charged particles accumulating on its surface), it is natural to assume that changes in the I_{ds} gradient reflect the concentration of the target object, because the adsorption/accumulation rate varies depending on its concentration. To verify this assumption, we calculated and plotted the time-dependent gradients of the I_{ds}. Figure 25 shows the resulting time-dependent I_{ds} change rates. The obtained experimental results showed consistency between duplicate measurements, with the gradients of I_{ds} changes presenting the highest value under subthreshold bias voltage conditions.

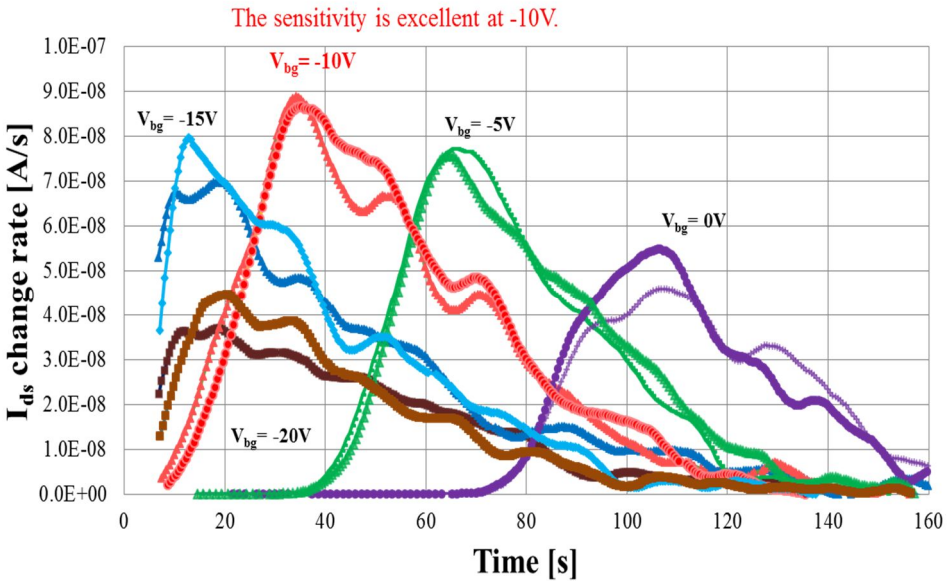

Figure 25. The conductance change rates versus time in each back-gate bias conditions.

Similar maximum gradients were exhibited at the turn-on region, with a peak *gm* at the depleted turn-off region, whereas the sensitivity was comparatively low under the full turn-on channel bias condition. This suggests that the amount of additional holes created in the nanochannel by the field-effect of chemical gating is less sensitive to the back-gate voltage, because of the saturation state reached under the full turn-on condition. Considering these results together, we can infer that the nanoFET sensor has its highest measurement sensitivity, with a peak g_m, in the subthreshold

region, whereas there are no noticeable sensitivity-related advantages or disadvantages in the region beyond the threshold voltage at off-level. This led to the conclusion that the bias of the ion concentration detector device should be configured using the gradient change at the initial I_{ds} level of 1 nA, given that the highest sensitivity of the sensor can be obtained with the subthreshold region bias conditions.

This may be considered the norm for back-gate bias voltage, because both the sensors detecting air anions, and the biosensors detecting the charges of protein molecules work based on the same principle. (V_{ds} = 1 V, Anions conc. ≈ 40,000 ea/cc.) Therefore, the detection sensitivity of a FET sensor may be defined as being the change in conductivity with respect to anionic concentration. It should be noted that in the subthreshold voltage region (0–5 V), the channel changes exhibit time delays with different onset times. This indicates that a sufficient number of electric charges must first accumulate on the sensor surface, to induce the channel turn on, proving again that back-gate modulation and chemical gating occur under similar conditions. The information for quantitative detection was reported such in the Conference KMEMS2015.

With a constant V_{bg} condition

Figure 26 shows the experimental results obtained for the nano FET sensor detection characteristics at various ion concentrations, under the bias voltage condition $V_{bg} = -10$ V (chosen for peak sensitivity). The experiment was conducted to test the ability of the device to detect anions in air and quantify their concentrations. Figure 26 displays the obtained real-time results for the I_{ds} dependence on the anionic concentration, and plots I_{ds}, as measured in real time.

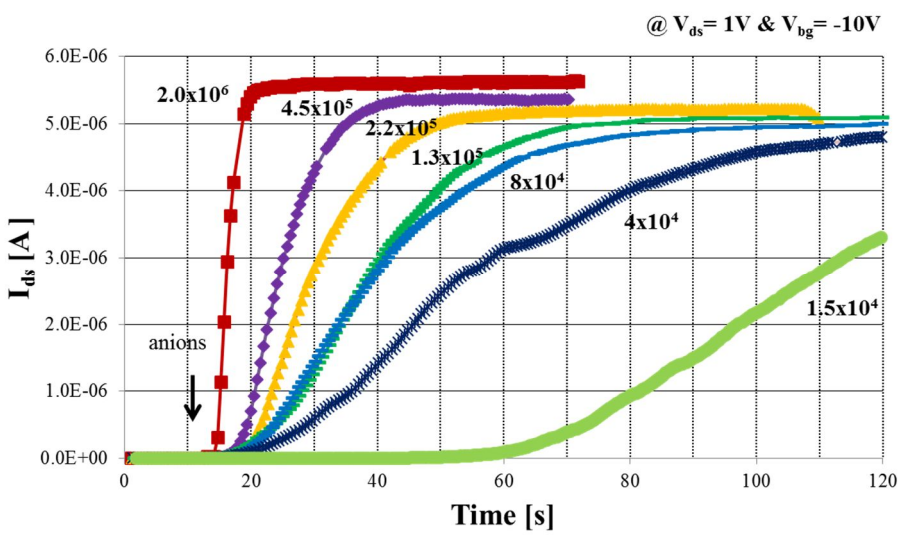

Figure 26. Real-time measurement of negative ions for several anionic concentrations.

The I_{ds} gradients were measured (as was done in Figure 26) immediately before and after the 11 s time point, for each anionic concentration in Figure 26. In accordance with the expected patterns, the higher the anionic concentration was, the greater the I_{ds} change gradient became, and the faster the saturation level was reached; as the anionic concentration decreased, the gradient of the I_{ds} change decreased, with this current slowly moving towards the saturation level.

.

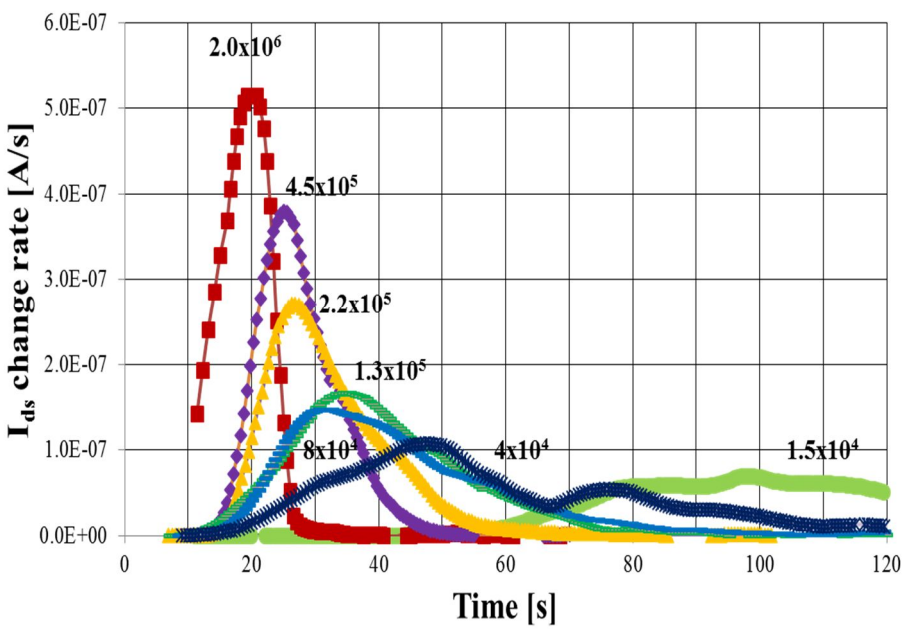

Figure 27. Plots of the slopes obtained from the I_{ds} change data.

This indicates that the nanoFET sensor can quantitatively detect the concentration of the object adsorbed on its surface, with the I_{ds} change rate (I_{ds} change expressed as an adsorption amount per hour) increasing with the increase in concentration, as can be verified by the maximum I_{ds} gradient. Furthermore, the peak I_{ds} value increases with an increasing concentration of the adsorbed detection, as confirmed by the several I_{ds} saturation levels shown in Figure 27. The maximum amount of adsorbed anions detectable by the nanoFET sensor, i.e., the maximum value of field-effect achieved at a given concentration of the detection object, has a positive correlation with the air anionic concentration. At low concentrations, even with enough time for adsorption, the maximum I_{ds} (at saturation level) cannot reach those of higher concentrations. From the experimental results, we can infer that I_{ds} converges towards a saturation level corresponding to a complete adsorption of all ionic charges in air. The saturation level, even once attained, still has room for a slight increase in anion adsorption on the sensor surface if the ionic concentration of the detection object is high. Figure 28 plots the maximum I_{ds} change rates for various air anionic concentrations (the air anionic concentration was measured with an ion counter). As shown in this figure, the air anionic concentration, when expressed on a log scale, is linearly related to the maximum I_{ds} rate.

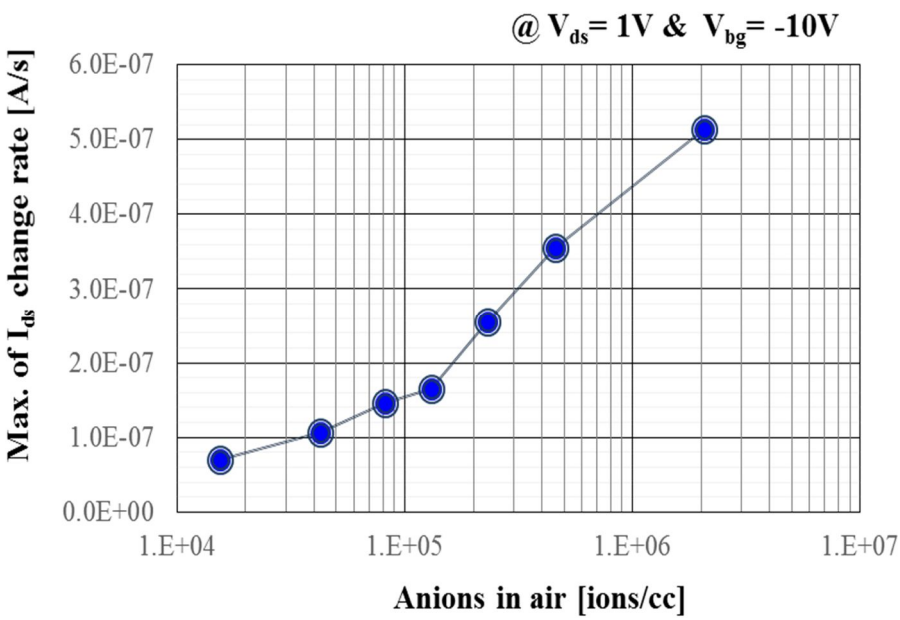

Figure 28. Maximum value of I_{ds} change rate for different anionic concentrations.

Comparison with a commercial ion counter

We compared the ion detection results obtained with the developed nanoFET sensor with a conventional ion counter; the comparison results are shown in Figure 29. Air anionic concentration measurements were simultaneously performed at the same location using the nanoFET sensor and the ion counter, at several distances of the ion generator. The right y-axis represents the air anionic concentration measured by the ion counter.

The left y-axis represents the maximum I_{ds} slopes obtained with the two nanoFETs. The negative ion concentrations measured by the ion counter (NT-C101A, Andes, Japan) at distances from the ion generator varying from 20 cm to 70 cm are shown Figure 29. The concentration values shown Figure 29 for the ion counter are the mean values of the results obtained during 1 minute of measurement. In Figure 29, the obtained minimum and maximum value are also represented. The right y-axis represents the maximum slope of I_{ds}, the response of the nanoFET to the anionic concentrations.

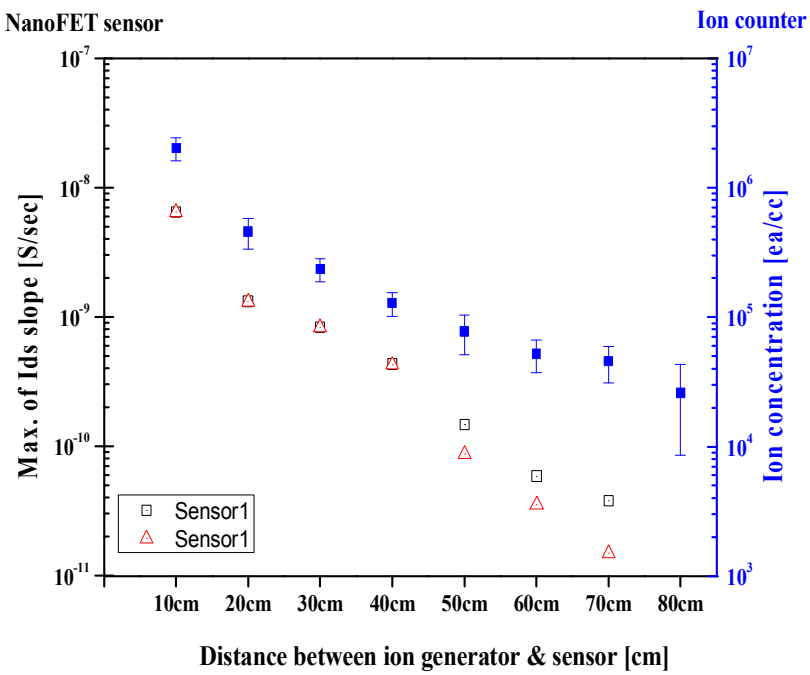

Figure 29. Comparison of the developed nanoFET sensor with a conventional airborne ion counter.

The experimental results obtained for the two different nanoFET sensor devices match well with each other, which clearly demonstrates the consistency of detection results obtained with nanoFET sensors. With the obtained experimental results for the nanoFET response and the air anions density counter results, for various distances between ion generator and the sensor device, the correlation between the nanoFET response and the anion quantification in air might be derived [65]. The nanoFET could detect anions with densities of negative ions as low as (approximately) 10^4 ea/cm^3. As previously discussed, the nanoFET sensors and air ion counter werein the same location, and performed simultaneous measurements (as shown in figure 30).

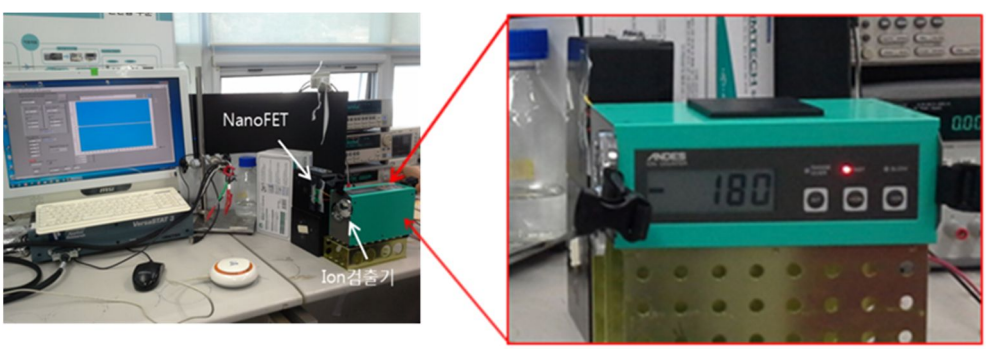

Figure 30. Images of experimental set-up to compare with a commercialized ion counter conventional ion counter.

4.3 Future works

A performance comparison of commercial anion counters is presented in Table 4. To allow for an exact comparison, measurements with these ion counters should be performed in the same exact environment; however, the data in this table for ion counters other than the NT-C101A and the nanoFET were provided by the manufacturing companies. Even though not a strict performance comparison, we have conducted an experiment under the same conditions, with the ion concentration measuring NT-C101A and the nanoFET sensor. The nanoFET prototype ion counter also contained the signal analysis circuit and a battery. The weight reported for the entire system is, thus, not accurately given in the table 4; it can, however, be produced with a total weight of less than 200 g. (without the housing it weights 40 g.) Additionally, we note that the minimum detectable ion density should be determined in extreme conditions, with no airflow; however, in this study, both the NT-C101A and nanoFET sensor were evaluated under (the same) normal atmospheric conditions. Both the NT-C101A and the proposed nanoFET performed similarly in our experimental conditions, concerning the minimum detectable ion density; given that the minimum detectable ion density of NT-C101A is 10 ions/cm^3, the minimum detectable ion density of our nanoFET ion counter can be assumed to have

the same value, and is presented as such in Figure 29. The value presented for the measuring range is also not accurate, because the air ionizer (Dr. USB, IMH Co. Korea) used in this experiments could not generate ion densities above 200×10^{4} ions/cm^{3}.

The suggested nanoFET sensor from this research, compare to the other existing commercialized negative ion sensors, is small volume, therefore intergration with other device and replacement of modulized nanoFET sensor can be strong advantage of commercialization. On the otherhand, inspection on ion in the air using nanoFET has no pervious research data, so there were a few experiments that checks the feasibility of quantitative ion detection with nanoFET. Before commercialization, to get an accurate evaluation of functionality such as the limit of detection, there needs to be a precise measurement in the standard for measuring methods of airborne ion density where the envirionment is not interffered by the external airflow.

Table 3. Recent state-of-the-art concerning ions detectors

	Japan			USA	Korea
	COM-3200	**COM-3600**	**NT-C101A**	**IC-1000-W**	**NanoFET**
Image					
Price	US$3231.47	US$10500	**US$2000**	US$1300	**(Less than) approx. $600**
Dimensions	W112xH45x D188(mm)	W100xH105x D250(mm)	**W70xD180xH110 (mm)**	W90xH160x D58(mm)	**In progress**
Weight	995g	2.5kg	**1.3Kg**	460g	**(Less than 200g)**
Minimum detectable ion density	10 (ions/cm^3)	1 (ions/cm^3)	**10 (ions/cm^3)**	100 (ions/cm^3)	**10 (ions/cm^3) ****
Measurable range	0-200×10^4 (ions/cm^3)	0-500×10^4 (ions/cm^3)	**10 -300×10^4 (ions/cm^3)**	10×10^4 - 2000×10^4 (ions/cm^3)	**10 -200×10^4 (ions/cm^3)****
Detectable mobility	Ranges of small ions : 0.4-0.8 (cm^2/Vs)	Ranges of small ions : 0.4-0.8 (cm^2/Vs)	**Ranges of small ions : 0.4-0.8 (cm^2/Vs)**	Ranges of small ions : 0.4-0.8 (cm^2/Vs)	**Ranges of small ions : 0.4-0.8 (cm^2/Vs)**
Measurement method	Gerdien capacitor method	Gerdien capacitor method	**Gerdien capacitor method**	Parallel flat plates method	**NanoFET**
Continuous ion measurement for 2–3 days	Not Good	Good	**Not Good**	Not Good	**Good (over 7days)**

** The precise test to be additionally conducted in the same environment by the standard for measuring methods of airborne ion density.

4.4 Summary

In summary, we developed and built nanoFET sensors for quantitative anion detection in the air. With the anion detection experiments at constant concentration, we have empirically shown that the sensitivity of the nano-FET biosensor is best in the subthreshold regime. Additionally, we successfully characterized the quantitative response for various anionic concentrations, by analyzing the slope of I_{ds}. The anions adsorbed on the sensor surface induce gate potential, a phenomenon called chemical gating; as a result, the conductance of the p-type nanoFET channel increases as the amount of the adsorbed anions increase. This indicates that anions are accumulated on the sensor surface. The maximum amount of accumulated anions does not show high relative variations in the saturation regime; hence, quantitative analysis is performed by using the slope of I_{ds}. In other words, we can quantify anionic concentration using the I_{ds} slope for each concentration. The nanoFET sensor, when used as a biosensor to detect the charge of biomolecules in a solution, operates under the same operating principle; therefore, we believe that we can rely on it to effectively differentiate false signals in the biosensor experiment.

Chapter 5.
Conclusion

Firstly, we demonstrated the viability of the detection of anions in air using nano field-effect transistor (nanoFET) devices. We detected the concentration of negative ions in air quantitatively. The sensitivity of the device, $\Delta I/I_o$, reached values above 700. Consistency in repeated measurements is essential, to allow the use of nanoFETs as air anion detection sensors. Since the operational principle of these sensors lies in measuring the changes in channel conductance induced by the field-effect generated by accumulated electrical charges, it is necessary to remove residual charges of previously adsorbed anions, to reset the sensor to the baseline state, before performing new measurements. The nanoFET device for anion detection has a silicon channel with a dimension of 5 μm (w) × 5 μm (l) × 20 nm (t) and a gate oxide SiO_2 layer with 15 nm thickness on top of the channel. We also proposed and manufactured a device with a floating metal electrode structure formed on the top of the gate oxide, to be used as the sensing area, and measured and evaluated its characteristics. While the nanoFET device with gate oxide deposition only (without the additional top-gate electrode) retained the electrical charges of the anions adsorbed on its sensing channel surface, the nanoFET device with the floating gate

electrode could reset the charges accumulated on the gate surface to the baseline state by a V_{bg} sweep. We presented a nanoFET sensor with floating gate structure, and compared its detection characteristics, based on chemical gating, with those of a nanoFET device having only a gate oxide channel surface, a configuration which was been intensely researched to be used in biosensors, by performing air anion detection tests to both types. As the ion strength of anions in air increases, the amount of negatively charged particles adsorbed on the channel surface of the nanoFET sensor increases. We measured the characteristics of the nanoFET devices under the influence of this phenomenon. Air anions were generated using an ion generator, and the sensors were exposed to the selected species of ion among those produced by the ion generator. The proposed air ion detection device using nanoFET is suitable as a low-cost, small, and easily implementable sensor, because the nanoFET can be easily mass produced as an electrical signal measurement semiconductor device. The air ion sensor device was implemented with a hand-held configuration, to prove that simple manufacturing of this ion sensor is possible. The implemented device also contained the circuits required to drive the back-gate bias voltage and measure the conductance changes in the nanoFET sensor channel

The nanoFET sensor for air anion detection was designed and produced with 8-inch semiconductor process facilities. This device has a channel

structure similar to the one of the nanoFET-based biosensor. The nanoFET has a 20 nm thick silicon channel, and a 15 nm thick SiO_2 layer as gate oxide, for negative ions adsorption. The nanochannel for the sensing area was made with 5 μm in both length and width, by stepper photolithography.

We expect that our nanoFET sensor will foster further understanding of nanoFET biosensors, because it presents no noise or false signals induced by other interferences existing in the liquid environments. Further research is underway, to evaluate the limits on detection and dynamic range at different air anionic concentrations, and determine the reliability and measurement reproducibility required for commercialization.

Reference

[1] B. R. Li, C. C. Chen, U. R. Kumar, and Y. T. Chen, "Advances in nanowire transistors for biological analysis and cellular investigation," *Analyst,* vol. 139, pp. 1589-1608, 2014.

[2] K. I. Chen, B. R. Li, and Y. T. Chen, "Silicon nanowire field-effect transistor-based biosensors for biomedical diagnosis and cellular recording investigation," *Nano Today,* vol. 6, pp. 131-154, Apr 2011.

[3] F. Patolsky, G. F. Zheng, and C. M. Lieber, "Nanowire-based biosensors," *Analytical Chemistry,* vol. 78, pp. 4260-4269, Jul 1 2006.

[4] Y. L. Bunimovich, Y. S. Shin, W.-S. Yeo, M. Amori, G. Kwong, and J. R. Heath, "Quantitative real-time measurements of DNA hybridization with alkylated nonoxidized silicon nanowires in electrolyte solution," *Journal of the American Chemical Society,* vol. 128, pp. 16323-16331, 2006.

[5] G. F. Zheng, F. Patolsky, Y. Cui, W. U. Wang, and C. M. Lieber, "Multiplexed electrical detection of cancer markers with nanowire sensor arrays," *Nature Biotechnology,* vol. 23, pp. 1294-1301, Oct 2005.

[6] H. S. Im, X. J. Huang, B. Gu, and Y. K. Choi, "A dielectric-modulated field-effect transistor for biosensing," *Nature Nanotechnology,* vol. 2, pp. 430-434, Jul 2007.

[7] K. N. Lee, S. W. Jung, K. S. Shin, W. H. Kim, M. H. Lee, and W. K. Seong, "Fabrication of suspended silicon nanowire arrays," *Small,* vol. 4, pp. 642-648, May 2008.

[8] E. Buitrago, M. Fernandez-Bolanos, S. Rigante, C. F. Zilch, N. S. Schroter, A. M. Nightingale*, et al.*, "The top-down fabrication of a 3D-integrated, fully CMOS-compatible FET biosensor based on vertically stacked SiNWs and FinFETs," *Sensors and Actuators B-Chemical,* vol. 193, pp. 400-412, Mar 2014.

[9] C. H. Kim, J. H. Ahn, K. B. Lee, C. Jung, H. G. Park, and Y. K. Choi, "A New Sensing Metric to Reduce Data Fluctuations in a Nanogap-Embedded Field-Effect Transistor Biosensor," *IEEE Transactions on Electron Devices,* vol. 59, pp. 2825-2831, Oct 2012.

[10] J. N. Tey, I. P. M. Wijaya, J. Wei, I. Rodriguez, and S. G. Mhaisalkar, "Nanotubes-/nanowires-based, microfluidic-integrated transistors for detecting biomolecules," *Microfluidics and Nanofluidics,* vol. 9, pp. 1185-1214, Dec 2010.

[11] N. K. Rajan, K. Brower, X. X. Duan, and M. A. Reed, "Limit of detection of field effect transistor biosensors: Effects of surface modification and size dependence," *Applied Physics Letters,* vol. 104, Feb 24 2014.

[12] E. Stern, A. Vacic, N. K. Rajan, J. M. Criscione, J. Park, B. R. Ilic*, et al.*, "Label-free biomarker detection from whole blood," *Nature nanotechnology,* vol. 5, pp. 138-142, 2009.

[13] H. R. Byon, S. Kim, and H. C. Choi, "Label-Free Biomolecular Detection Using Carbon Nanotube Field Effect Transistors," *Nano,* vol. 3, pp. 415-431, Dec 2008.

[14] A. Kim, C. S. Ah, H. Y. Yu, J.-H. Yang, I.-B. Baek, C.-G. Ahn*, et al.*, "Ultrasensitive, label-free, and real-time immunodetection using silicon field-effect transistors," *Applied Physics Letters,* vol. 91, p. 3901, 2007.

[15] T. Kong, R. G. Su, B. B. Zhang, Q. Zhang, and G. S. Cheng, "CMOS-compatible, label-free silicon-nanowire biosensors to detect cardiac troponin I for acute myocardial infarction diagnosis," *Biosensors & Bioelectronics,* vol. 34, pp. 267-272, Apr 15 2012.

[16] N. Elfström, A. E. Karlström, and J. Linnros, "Silicon nanoribbons for electrical detection of biomolecules," *Nano letters,* vol. 8, pp. 945-949, 2008.

[17] S. Chen, L. Nyholm, N. Jokilaakso, A. E. Karlström, J. Linnros, U. Smith*, et al.*, "Current instability for silicon nanowire field-effect sensors operating in

electrolyte with platinum gate electrodes," *Electrochemical and solid-state letters,* vol. 14, pp. J34-J37, 2011.

[18] G. S. Kulkarni and Z. H. Zhong, "Detection beyond the Debye Screening Length in a High-Frequency Nanoelectronic Biosensor," *Nano Letters,* vol. 12, pp. 719-723, Feb 2012.

[19] E. Stern, A. Vacic, C. Li, F. N. Ishikawa, C. W. Zhou, M. A. Reed*, et al.*, "A Nanoelectronic Enzyme-Linked Immunosorbent Assay for Detection of Proteins in Physiological Solutions," *Small,* vol. 6, pp. 232-238, Jan 18 2010.

[20] A. Kim, C. S. Ah, C. W. Park, J. H. Yang, T. Kim, C. G. Ahn*, et al.*, "Direct label-free electrical immunodetection in human serum using a flow-through-apparatus approach with integrated field-effect transistors," *Biosensors & Bioelectronics,* vol. 25, pp. 1767-1773, Mar 15 2010.

[21] E. Stern, R. Wagner, F. J. Sigworth, R. Breaker, T. M. Fahmy, and M. A. Reed, "Importance of the debye screening length on nanowire field effect transistor sensors," *Nano Letters,* vol. 7, pp. 3405-3409, Nov 2007.

[22] A. R. Gao, N. Lu, Y. C. Wang, P. F. Dai, T. Li, X. L. Gao*, et al.*, "Enhanced Sensing of Nucleic Acids with Silicon Nanowire Field Effect Transistor Biosensors," *Nano Letters,* vol. 12, pp. 5262-5268, Oct 2012.

[23] J. H. Ahn, J. Y. Kim, K. Choi, D. I. Moon, C. H. Kim, M. L. Seol*, et al.*, "Nanowire FET Biosensors on a Bulk Silicon Substrate," *IEEE Transactions on Electron Devices,* vol. 59, pp. 2243-2249, Aug 2012.

[24] M. S. Makowski and A. Ivanisevic, "Molecular Analysis of Blood with Micro-/Nanoscale Field-Effect-Transistor Biosensors," *Small,* vol. 7, pp. 1863-1875, Jul 18 2011.

[25] C. P. Chen, A. Ganguly, C. Y. Lu, T. Y. Chen, C. C. Kuo, R. S. Chen*, et al.*, "Ultrasensitive in Situ Label-Free DNA Detection Using a GaN Nanowire-Based Extended-Gate Field-Effect-Transistor Sensor," *Analytical Chemistry,* vol. 83, pp. 1938-1943, Mar 15 2011.

[26] E. Stern, A. Vacic, N. K. Rajan, J. M. Criscione, J. Park, B. R. Ilic*, et al.*, "Label-free biomarker detection from whole blood," *Nature Nanotechnology,* vol. 5, pp. 138-142, Feb 2010.

[27] E. Stern, A. Vacic, and M. A. Reed, "Semiconducting Nanowire Field-Effect Transistor Biomolecular Sensors," *IEEE Transactions on Electron Devices,* vol. 55, pp. 3119-3130, Nov 2008.

[28] E. Stern, J. F. Klemic, D. A. Routenberg, P. N. Wyrembak, D. B. Turner-Evans, A. D. Hamilton*, et al.*, "Label-free immunodetection with CMOS-compatible semiconducting nanowires," *Nature,* vol. 445, pp. 519-522, Feb 1 2007.

[29] S. Boussaad, B. A. Diner, and J. Fan, "Influence of redox molecules on the electronic conductance of single-walled carbon nanotube field-effect transistors: Application to chemical and biological sensing," *Journal of the American Chemical Society,* vol. 130, pp. 3780-3787, Mar 26 2008.

[30] C. C. Yu, S. W. Lee, J. Ong, D. Moore, and R. F. Saraf, "Single Electron Transistor in Aqueous Media," *Advanced Materials,* vol. 25, pp. 3079-3084, Jun 11 2013.

[31] M. Rouhanizadeh, W. Takabe, L. S. Ai, H. Y. Yu, and T. Hsiai, "Monitoring oxidative stress in vascular endothelial cells in response to fluid shear stress: From biochemical analyses to micro- and Nanotechnologies," *Nitric Oxide, Pt G: Oxidative and Nitrosative Stress in Redox Regulation of Cell Signaling,* vol. 441, pp. 111-150, 2008.

[32] M. Curreli, R. Zhang, F. N. Ishikawa, H. K. Chang, R. J. Cote, C. Zhou*, et al.*, "Real-Time, Label-Free Detection of Biological Entities Using Nanowire-Based FETs," *IEEE Transactions on Nanotechnology,* vol. 7, pp. 651-667, Nov 2008.

[33] Y. Cui, Q. Q. Wei, H. K. Park, and C. M. Lieber, "Nanowire nanosensors for highly sensitive and selective detection of biological and chemical species," *Science,* vol. 293, pp. 1289-1292, Aug 17 2001.

[34] W. H. Guan, N. K. Rajan, X. X. Duan, and M. A. Reed, "Quantitative probing of surface charges at dielectric-electrolyte interfaces," *Lab on a Chip,* vol. 13, pp. 1431-1436, 2013.

[35] A. Vacic, J. M. Criscione, E. Stern, N. K. Rajan, T. Fahmy, and M. A. Reed, "Multiplexed SOI BioFETs," *Biosensors & Bioelectronics,* vol. 28, pp. 239-242, Oct 15 2011.

[36] J. M. Blatny, B. A. P. Reif, G. Skogan, O. Andreassen, E. A. Høiby, E. Ask*, et al.*, "Tracking airborne Legionella and Legionella pneumophila at a biological treatment plant," *Environmental science & technology,* vol. 42, pp. 7360-7367, 2008.

[37] U. Horrak, J. Salm, and H. Tammet, "Statistical characterization of air ion mobility spectra at Tahkuse Observatory: Classification of air ions," *Journal of Geophysical Research: Atmospheres (1984–2012),* vol. 105, pp. 9291-9302, 2000.

[38] F. Sulman, "The impact of weather on human health," *Reviews on environmental health,* vol. 4, pp. 83-119, 1983.

[39] A. P. Krueger and E. J. Reed, "Biological Impact of Small Air Ions," *Science,* vol. 193, pp. 1209-1213, 1976.

[40] A. P. Krueger and R. F. Smith, "The Biological Mechanisms of Air Ion Action I. 5-Hydroxytryptamine as the endogenous mediator of positive air ion effects on the mammalian trachea," *The Journal of general physiology,* vol. 43, pp. 533-540, 1960.

[41] A. P. Krueger and R. F. Smith, "The Biological Mechanisms of Air Ion Action II. Negative air ion effects on the concentration and metabolism of 5-hydroxytryptamine in the mammalian respiratory tract," *The Journal of general physiology,* vol. 44, pp. 269-276, 1960.

[42] L. A. Fletcher, L. F. Gaunt, C. B. Beggs, S. J. Shepherd, P. A. Sleigh, C. J. Noakes*, et al.*, "Bactericidal action of positive and negative ions in air,"

BMC microbiology, vol. 7, p. 32, 2007.

[43] L. Livanova, I. Levshina, L. Nozdracheva, M. Elbakidze, and M. Airapetyants, "The protective effects of negative air ions in acute stress in rats with different typological behavioral characteristics," *Neuroscience and behavioral physiology,* vol. 29, pp. 393-395, 1999.

[44] E. A. Kosenko, Y. G. Kaminsky, I. G. Stavrovskaya, T. V. Sirota, and M. N. Kondrashova, "The stimulatory effect of negative air ions and hydrogen peroxide on the activity of superoxide dismutase," *Febs Letters,* vol. 410, pp. 309-312, Jun 30 1997.

[45] Y. S. Kim, K. Y. Yoon, J. H. Park, and J. Hwang, "Application of air ions for bacterial de-colonization in air filters contaminated by aerosolized bacteria," *Science of the total environment,* vol. 409, pp. 748-755, 2011.

[46] C. W. Park, J. W. Park, S. H. Lee, and J. Hwang, "Real-time monitoring of bioaerosols via cell-lysis by air ion and ATP bioluminescence detection," *Biosensors & Bioelectronics,* vol. 52, pp. 379-383, Feb 15 2014.

[47] T. Reilly and I. Stevenson, "An investigation of the effects of negative air ions on responses to submaximal exercise at different times of day," *Journal of human ergology,* vol. 22, pp. 1-9, 1993.

[48] J. H. Chua, R.-E. Chee, A. Agarwal, S. M. Wong, and G.-J. Zhang, "Label-free electrical detection of cardiac biomarker with complementary metal-oxide semiconductor-compatible silicon nanowire sensor arrays," *Analytical chemistry,* vol. 81, pp. 6266-6271, 2009.

[49] S. Kim, K. Cho, K. Kwak, and S. Kim, "Memory Characteristics of Doubly Stacked Nano-Floating Gate Memory Devices with Channels of Single ZnO Nanowires," *Journal of Nanoscience and Nanotechnology,* vol. 13, pp. 6196-6198, Sep 2013.

[50] P. C. Chen, G. Z. Shen, and C. W. Zhou, "Chemical Sensors and Electronic Noses Based on 1-D Metal Oxide Nanostructures," *IEEE Transactions on*

Nanotechnology, vol. 7, pp. 668-682, Nov 2008.

[51] W. Lu and C. M. Lieber, "Nanoelectronics from the bottom up," *Nature Materials,* vol. 6, pp. 841-850, Nov 2007.

[52] L. J. Lauhon, M. S. Gudiksen, and C. M. Lieber, "Semiconductor nanowire heterostructures," *Philosophical Transactions of the Royal Society of London Series a-Mathematical Physical and Engineering Sciences,* vol. 362, pp. 1247-1260, Jun 15 2004.

[53] G. Lehoucq, P. Bondavalli, S. Xavier, P. Legagneux, P. Abbyad, C. N. Baroud*, et al.*, "Highly sensitive pH measurements using a transistor composed of a large array of parallel silicon nanowires," *Sensors and Actuators B-Chemical,* vol. 171, pp. 127-134, Aug-Sep 2012.

[54] H. Geiger and W. Müller, "Elektronenzählrohr zur messung schwächster aktivitäten," *Naturwissenschaften,* vol. 16, pp. 617-618, 1928.

[55] N. Shinohara, M. Tokumura, M. Kazama, H. Yoshino, S. Ochiai, and A. Mizukoshi, "Indoor air quality, air exchange rates, and radioactivity in new built temporary houses following the Great East Japan Earthquake in Minamisoma, Fukushima," *Indoor Air,* vol. 23, pp. 332-341, Aug 2013.

[56] M. A. Noras, B. T. Williams, and J. Kieres, "A novel ion monitoring device," *Journal of electrostatics,* vol. 63, pp. 533-538, 2005.

[57] Y.-T. Seo, K.-N. Lee, K. J. Jang, M.-H. Lee, H. Lee, W. Seong*, et al.*, "Negative ions detection in air using nano field-effect-transistor (nanoFET)," *Micro and Nano Systems Letters,* vol. 2, pp. 1-6, 2014.

[58] A. Al Naim, A. Hobson, R. T. Grant, A. Dragoneas, M. Hampton, C. Dunscombe*, et al.*, "Water-gated organic nanowire transistors," *Organic Electronics,* vol. 14, pp. 1057-1063, Apr 2013.

[59] D. R. Kim, C. H. Lee, and X. L. Zheng, "Probing Flow Velocity with Silicon Nanowire Sensors," *Nano Letters,* vol. 9, pp. 1984-1988, May 2009.

[60] B. R. Li, C. W. Chen, W. L. Yang, T. Y. Lin, C. Y. Pan, and Y. T. Chen,

"Biomolecular recognition with a sensitivity-enhanced nanowire transistor biosensor," *Biosensors & Bioelectronics,* vol. 45, pp. 252-259, Jul 15 2013.

[61] S. Sorgenfrei, C. Y. Chiu, M. Johnston, C. Nuckolls, and K. L. Shepard, "Debye Screening in Single-Molecule Carbon Nanotube Field-Effect Sensors," *Nano Letters,* vol. 11, pp. 3739-3743, Sep 2011.

[62] N. Elfstrom, A. E. Karlstrom, and J. Linnrost, "Silicon nanoribbons for electrical detection of biomolecules," *Nano Letters,* vol. 8, pp. 945-949, Mar 2008.

[63] M. H. Sorensen, N. A. Mortensen, and M. Brandbyge, "Screening model for nanowire surface-charge sensors in liquid," *Applied Physics Letters,* vol. 91, Sep 3 2007.

[64] L. Fletcher, C. Noakes, P. Sleigh, C. Beggs, and S. Shepherd, "Air ion behavior in ventilated rooms," *Indoor and Built Environment,* vol. 17, pp. 173-182, 2008.

[65] X. Duan, Y. Li, N. K. Rajan, D. A. Routenberg, Y. Modis, and M. A. Reed, "Quantification of the affinities and kinetics of protein interactions using silicon nanowire biosensors," *Nature nanotechnology,* vol. 7, pp. 401-407, 2012.

Abstract(Korean)

본 논문은 처음으로 top-dowm 방식으로 제작된 NanoFET를이용하여 공기중의 음이온을 정량적으로 검출 하였다. 또한 나노 전계효과트렌지스터(nanoFET)를 제작하고 소자의 나노 채널표면에서의 전하의 charge의하여 발생하는 전계효과로 달라지는 채널 conductance의 변화를 측정함으로 동작 원리를 실험적으로 규명하는데 의의가 있다. 일반적인 nanoFET 실험에서 발생하는 버퍼 용액의 이온 농도, pH 농도 그리고 용액의 포텐셜에 의한 간섭을 비롯한 여러 노이즈 신호 때문에 센서개발에 어려움이 많았다. 하지만 본 연구에서 제안한 nanoFET를 이용한 공기중 음이온 측정 방법은 전하를 띤 입자의 흡착에 의한 chemical gate현상이 동작 원리로써 명확하게 설명할 수 있다. 또한 공기중 음이온을 측정하는 기존 상용화 장비와 성능평가를 통해 nanoFET를 이용한 공기 음이온 센서의 상용화 가능성을 확인하였다.

기존 공기 중 음이온 측정 방법은 공기를 빨아들이는 송풍구와 Gerdien tube를 이용하여 공기중 입자들의 음전하에 의하여 달라지는 전기장을 측정하는 방식이다. 상용화된 Gerdien tube을 이용한 공기중 음이온 측정장비는 nanoFET와 비교하여 부피가 상대적으로 크다. 또한 최근 일상 생활 기기들로 응용되는 음이온 발생기나 공기의 질을 평가할 수 있는 다른 기기들과의 직접화가 어렵다는 단점이 있다. nanoFET를 이용한 음이온 측정 방식을 기존 공기청정기, 선풍기, 냉장고 등과 같은 소형 가전제품들의 음이온 공급장치와 직접화를 이룬다면 공기중 음이온을 효과적으로 제어하여 건강한 일상생활과 공기의 질을 관리 할 수 있는 지표기기로

사용이 가능하다.

또한 nanoFET에 대한 연구분야 가운데 제작공정에 관한 연구가 지속되었다. 초반에는 nanowire와 carbon nanotube의 전기적 특성을 비롯하여 기본특성에 초점이 맞추어졌다. 때문에 the bottom-up approach 방법을 이용한 nanoFET 센서개발에 대한 가능성을 확인 하는 연구가 진행되어왔다. 초기의 nanoFET연구가 nanowire와 CNT 기본 특성에 초점이 맞추어졌다면, 현재는 상용화 소자개발을 위하여 재현성과 대량생산이 가능한 공정방법에 대한 연구가 진행되고 있다. 아무리 우수한 SWCNT나 single crystal nanowire를 이용한 소자라고 할지라도 기판에 분산시키고 전극을 형성하는 과정에서 생산성이 top-down approach 에 비하여 떨어지게 된다. 지금까지 보고된 top-down approach 방법은 silicon wafer의 결정방향에 따라 wet-etch 공정으로 nanowire 구조를 제작한 후에 source, drain, gate 전극을 제작하여 균일한 nanochannel의 길이와 신호의 재현성에 초점을 두어 연구가 진행되었다. 이와 같은 기존 top-down approach로 제작한 소자들도 상용화 센서를 제작하기에는 공정의 까다로움과 소자 제작 수율이 극복해야 할 문제점이다.

본 논문에서는 복잡한 nanoFET 제작공정을 일반적인 MEMS 공정을 이용하여 8인치 ultra-thin silicon-on-insulator (UT-SOI) wafer에 nanoFET의 채널에서부터 표면처리까지의 일괄공정을 대량생산이 가능하도록 간단하게 구현하였다. 나노채널, gate oxide, floating gate electrode (Ti/Au), 그리고 BOX silicon layer가 각각 20, 15, 10/100, and 145 nm이다. 또한 채널의 길

이와 선폭은 5μm, 1 μm 로 제작 되었다. 제작된 nanoFET의 채널에 흡착된 전하를 띤 입자들의 흡착에 의하여 chemical gate 현상을 측정 결과로 확인 하였다.

특히, 공기 중 음이온의 다양한 농도에 대한 nanoFET의 동작 특성을 반복 측정하여 채널표면에 흡착된 전하가 chemical gatting 현상에 의하여 동작함을 실험적으로 명확하게 규명하였다. 음이온 발생기로부터 공기 중 음이온의 확산을 통해 소자의 검출영역인 gate표면에 흡착되었을 때의 전류(I_{ds})값의 변화를 측정값의 기울기 값으로 측정함으로 정량적인 분석을 하였다. nanoFET의 게이트 산화막 위에 추가적인 top-gate gold 전극을 도입함으로 소자의 감지영역을 넓히고, 전하의 축적(the charges accumulated)을 초기화 할 수 있기 때문에 공기 중 음이온 센서로써 활용 효율을 개선하였다. 이런 원리로 게이트 전극을 갖고 있는 nanoFET 센서는 반복적으로 측정가능한 공기중 음이온 측정 센서로 활용 가능할 것으로 기대된다.

주요어: 공기중 음이온, 음이온의 감지, 나노전계효과트랜지스터, 화학적 게이트, 전도도변화율, 멤스(MEMS)

학 번: 2007-30828